Cathepsin-Targeting SARS-CoV-2 Inhibitors: Design, Synthesis, and Biological Activity

Philipp Flury,[a,≠] Julian Breidenbach,[b,≠] Nadine Krüger,[c,≠] Rabea Voget,[b] Laura Schäkel,[b] Yaoyao Si,[b] Vesa Krasniqi,[b] Sara Calistri,[a] Matthias Olfert,[a] Katharina Sylvester,[b] Cheila Rocha,[c] Raphael Ditzinger,[a] Alexander Rasch,[a] Stefan Pöhlmann,[c,d] Thales Kronenberger,[a,e,f] Antti Poso,[a,e] Katharina Rox,[g,h] Stefan A. Laufer,[a] Christa E. Müller,[b] Michael Gütschow,[b,*] and Thanigaimalai Pillaiyar[a,*]

[a]Institute of Pharmacy, Pharmaceutical/Medicinal Chemistry and Tübingen Center for Academic Drug Discovery, Eberhard Karls University Tübingen, Auf der Morgenstelle 8, 72076 Tübingen, Germany

[b]PharmaCenter Bonn, Pharmaceutical Institute, Pharmaceutical & Medicinal Chemistry, University of Bonn, An der Immenburg 4, 53121 Bonn, Germany

[c]Infection Biology Unit, German Primate Center, Leibniz Institute for Primate Research Göttingen, Kellnerweg 4, 37077 Göttingen, Germany

[d]Faculty of Biology and Psychology, University Göttingen, Göttingen 37073, Germany

[e]School of Pharmacy, University of Eastern Finland, Faculty of Health Sciences, Kuopio 70211, Finland

[f]Excellence Cluster "Controlling Microbes to Fight Infections" (CMFI), 72076 Tübingen, Germany

[g]Department of Chemical Biology, Helmholtz Centre for Infection Research (HZI), 38124 Braunschweig, Germany

[h]German Center for Infection Research (DZIF), Partner Site Hannover-Braunschweig, 38124 Braunschweig, Germany

ABSTRACT: Cathepsins (Cats) are proteases that mediate the successful entry of SARS-CoV-2 into host cells. We designed and synthesized a tailored series of 21 peptidomimetics and evaluated their inhibitory activity against human cathepsins L, B, and S. Structural diversity was realized by combinations of different C-terminal warhead functions and N-terminal capping groups, while a central Leu-Phe fragment was maintained. Several compounds were identified as promising cathepsin L and S inhibitors with K_i values in the low nanomolar to subnanomolar range, for example, the peptide aldehydes **9a** and **9b** (**9a**, 2.67 nM, CatL; 0.0455 nM, CatS; **9b**, 1.76 nM, CatL; 0.0512 nM, CatS). The compounds' inhibitory activity against the main protease of SARS-CoV-2 (M^{pro}) was additionally investigated. Based on the results at CatL, CatS, and M^{pro}, selected inhibitors were subjected to investigations of their antiviral activity in cell-based assays. In particular, the peptide nitrile **11e** exhibited promising antiviral activity with an EC_{50} value of 35.1 nM in Calu-3 cells without showing cytotoxicity. High metabolic stability and favorable pharmacokinetic properties make **11e** suitable for further preclinical development.

KEYWORDS: *COVID-19, cathepsin inhibitors, main protease, peptidomimetics, SARS-CoV-2, viral entry.*
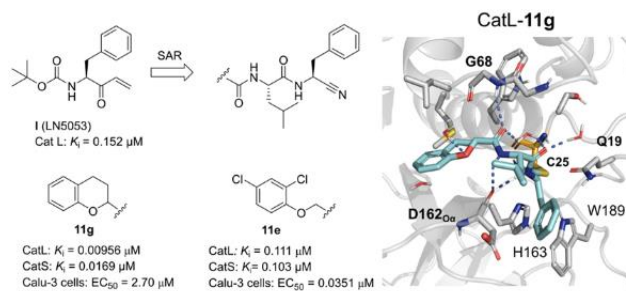
1. INTRODUCTION

The novel severe acute respiratory syndrome coronavirus-2 (SARS-CoV-2) is a beta-coronavirus, which is the causative agent for coronavirus disease 19 (COVID-19), a respiratory global pandemic that emerged in 2019. After three years of the pandemic, over 760 million people have been infected, and around 6.9 million have died.[1] Prophylactic and therapeutic

intervention strategies are still urgently required because the COVID-19 pandemic presents an unprecedented challenge to public health.

More than 20 different SARS-CoV-2 vaccines were tested and are currently in use. However, vaccine hesitancy still exists on a global scale, and breakthrough infections are frequent among vaccine recipients. Therefore, in the battle against COVID-19, developing specific antiviral drugs for SARS-CoV-2 is a top goal, especially with the rise of mutations that may partially evade neutralization by antibodies.[1] A variety of SARS-CoV-2 inhibitors have already been reported.[2-5] However, only few direct-acting antivirals, such as remdesivir, molnupiravir, and nirmatrelvir (Figure 1), have been approved. Remdesivir is an intravenously administered RNA-dependent RNA polymerase (RdRp) inhibitor for COVID-19 infection,[6] while molnupiravir is an orally available RdRp inhibitor used for the treatment of mild to moderate cases of COVID-19. It should be noted that remdesivir as well as molnupiravir are repurposed drugs.[6,7] Nirmatrelvir, a peptidomimetic inhibitor of the SARS-CoV-2 main protease (M^{pro}), is commercialized under the brand name Paxlovid in combination with ritonavir to prevent its fast metabolic degradation.[8] The cysteine protease M^{pro}, crucial for virus replication, is highly conserved across coronaviruses but lacks a close homolog in humans. Following the approval of Paxlovid, numerous compounds that inhibit M^{pro} have been reported.[9-17]
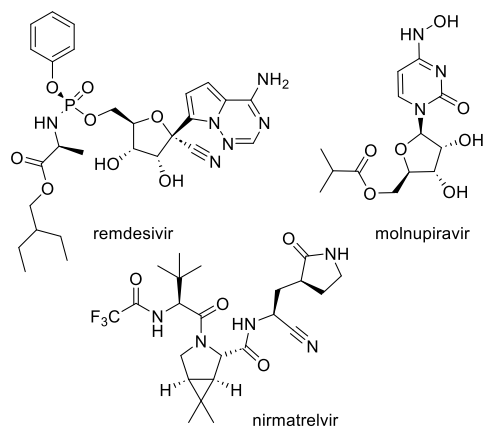
Figure 1. Structures of approved SARS-CoV-2 inhibitors for the treatment of COVID-19.

The SARS-CoV-2 virus is an enveloped positive-stranded RNA virus that exhibits remarkable genetic similarities to earlier coronaviruses, especially SARS-CoV-1, which first appeared in the Guangdong province, China, in 2002, and shares 79% of its genome.[18] It is now acknowledged that these two coronaviruses have similar molecular mechanisms for recognizing, entering, and replicating in hosts.[19-21]

SARS-CoV-2 entry into host cells depends on the interaction between the receptor-binding domain of the spike glycoprotein (S) and the cellular receptor of the host, *i.e.*, angiotensin-converting enzyme 2 (ACE2). The S1 and S2 subunits, which facilitate membrane fusion and attachment to host cells, are present in each monomeric unit of the S protein. The successful entry of the virus is dependent on the cleavage and activation of its spike protein by host cell proteases. The membrane-bound transmembrane serine protease 2

(TMPRSS2) is the main processing enzyme whose activity promotes direct endocytic cell entry via membrane fusion of the virus and the host cell.[21] The endosomal entry constitutes an alternative route of virion uptake. It is followed by S protein priming within the S1 domain, a process that occurs in the acidic endosomal-lysosomal compartment, where TMPRSS2 is not catalytically competent. Here, the cleavage of the SARS-CoV-2 S protein is catalyzed by human lysosomal cathepsins (Cats).[22-27] In particular, CatL has a crucial role in SARS-CoV-2 infection. It effectively cleaves the SARS-CoV-2 S protein, enhancing virus entry.[28]

Overexpression of CatL during COVID-19 was correlated with the progression and severity of the disease. Furthermore, the expression of CatL was upregulated by interleukin-6 (IL-6), a surrogate proinflammatory marker for severe COVID-19 disease with a poor prognosis.[28,29] This dual role in the viral entry and the progression of excessive COVID-19 pathology led to the recognition of cathepsins as targets against SARS-CoV-2. Noteworthy, in the Omicron variant of SARS-CoV-2, spike region mutations to basic amino acids caused reduced spike cleavage by TMPRSS2 and thus a decrease in direct host cell entry via membrane fusion. This is compensated by the increased use of the endosomal entry pathway and consequent cleavage by cathepsins.[30]

Several inhibitors targeting cathepsins have been reported for their anti-SARS-CoV-2 activity and have been proposed as a possible therapeutic option to combat COVID-19 (Figure 2). The pan-cathepsin inhibitor E-64d prevented the SARS-CoV-2-S-driven cell entry when it was co-administered with the TPMRSS2 inhibitor camostat mesylate.[21] The highly potent CatS/L inhibitor K777 and the picomolar cathepsin L inhibitor gallinamide A reduced SARS-CoV-2 infections in a number of cell lines. Both, K777 and gallinamide A, were inactive against M^{pro}.[24,25] The fluoromethylketone Z-FA-FMK, a potent, irreversible inhibitor of a number of cysteine proteases, including cathepsins B, L, and S, with less pronounced activity against M^{pro},[31] has demonstrated excellent anti-SARS-CoV-2 activity *in vitro* and *in vivo*.[32] Moreover, the strong cathepsin inhibitor calpeptin, a Z-protected leucine-norleucine-derived aldehyde, was active in SARS-CoV-2-treated hamsters.[33]
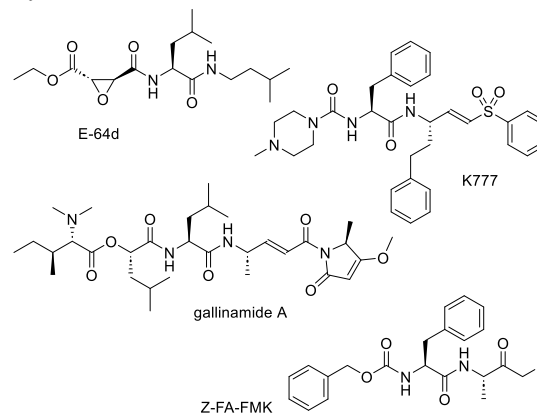
Figure 2. Structures of representative cathepsin-targeting SARS-CoV-2 inhibitors.
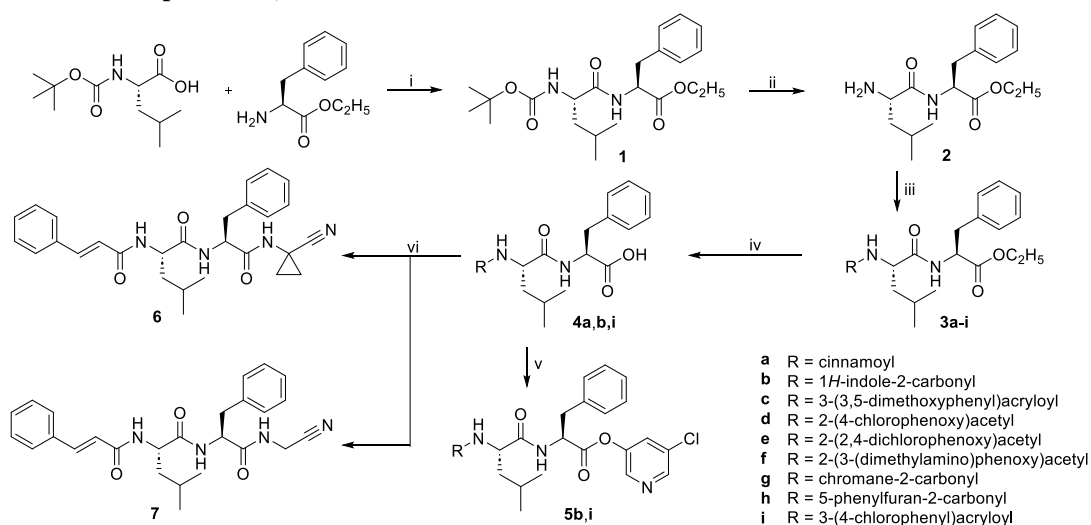
2
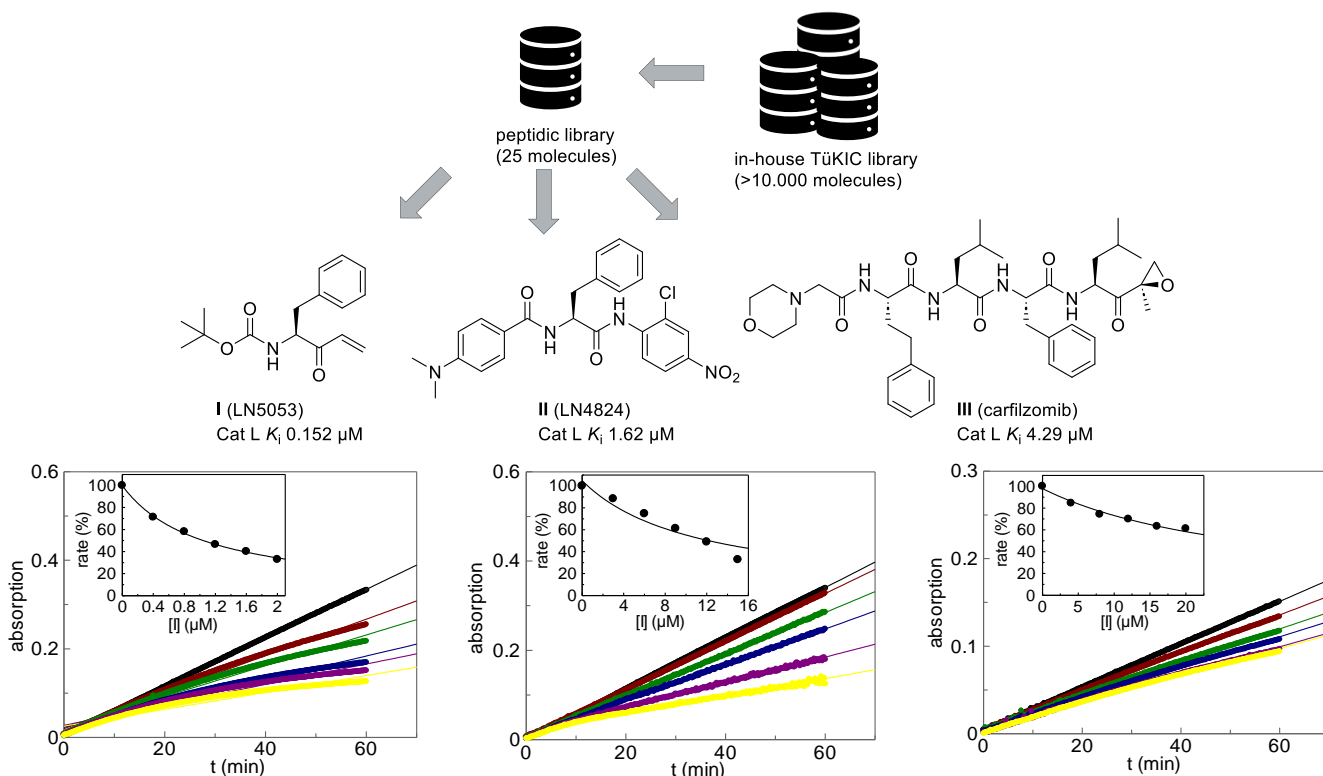
Figure 3. CatL inhibitory activity of hit compounds **I**-**III**, identified through high-throughput screening.

The growing appeal of cathepsins as therapeutic targets for COVID-19 served as the impetus for our research. In the present study, initiated by a virtual screening of the Tübingen Kinase Inhibitor Collection (TüKIC) for inhibition of CatL, we designed and synthesized a series of tailored peptidomimetics and characterized their inhibitory activity against CatL, B, S, and M[pro]. We discovered highly potent inhibitors, and based on these findings, their antiviral activity was determined. Docking studies were performed to obtain insights into their molecular interaction with the target protease CatL. Furthermore, the metabolic stability of the test compounds was investigated and demonstrated.

Scheme 1. Synthesis of Compounds 5b, 5i, **6**, **7**[a]

a R = cinnamoyl
b R = 1*H*-indole-2-carbonyl
c R = 3-(3,5-dimethoxyphenyl)acryloyl
d R = 2-(4-chlorophenoxy)acetyl
e R = 2-(2,4-dichlorophenoxy)acetyl
f R = 2-(3-(dimethylamino)phenoxy)acetyl
g R = chromane-2-carbonyl
h R = 5-phenylfuran-2-carbonyl
i R = 3-(4-chlorophenyl)acryloyl

[a]Reagents and conditions: (i) HATU, DIPEA, DMF (dry), 0→25 °C, 67%; (ii) 4M HCl in dioxane, CH₂Cl₂ (dry) 0→25 °C, 100%; (iii) carboxylic acid, HATU, DIPEA, DMF (dry), 0→25 °C, 55-90%; (iv) 2M aq. NaOH, MeOH, 25 °C, 73-97%; (v) 3-chloro-5-hydroxypyridine, HATU, DIPEA, DMF (dry), 0→25 °C, 11-59%; (vi) corresponding aminonitrile, HATU, DIPEA, DMF (dry), 0→25°C, 22-64%.
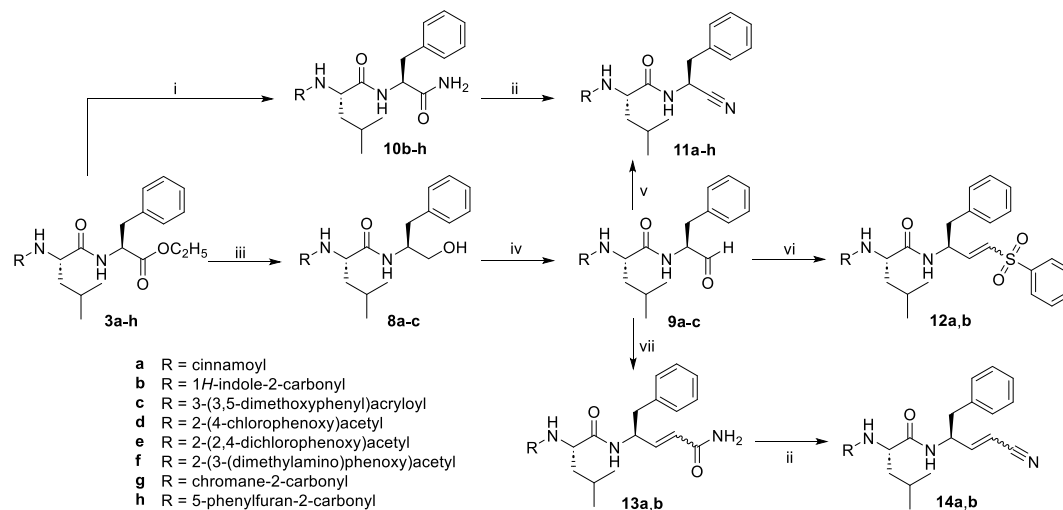
3

2. RESULTS AND DISCUSSION

2.1. Identification of hit molecules from virtual screening.

We compiled a small peptidic library from the collection of TüKIC, which contains over 10,000 members that target a nucleophilic cysteine residue in a variety of kinases. Initially, compounds were screened at 10 μM against CatL, and three hit compounds that inhibited CatL by ≥50% were chosen to examine concentration-dependent inhibition. The Michael acceptor **I** (Figure 3) inhibited CatL with a K_i value of 0.152 μM, while the nitroaniline derivative **II** and the proteasome inhibitor carfilzomib (**III**) showed moderate activity with K_i values of 1.62 and 4.29 μM, respectively. Compound **II** was previously reported as a covalent reversible inhibitor of SARS-CoV-1 M^pro with an IC_{50} value of 30 nM.[34] With the structural information from these hits and by particularly using compound **I** as a lead CatL inhibitor, we designed and synthesized new representatives of this chemotype by systematically incorporating various warhead groups and extending the lead structure at the N-terminus. The biochemical data of the generated series of peptidomimetics were analyzed, and structure-activity relationships (SARs) were deduced.

2.2. Chemistry.

The synthetic route to the final compounds **5**-**7** is outlined in Scheme 1. The peptidic fragment **1** was initially synthesized from Boc-protected L-leucine and L-phenylalanine ethyl ester using a HATU-mediated coupling in the presence of diisopropylethylamine (DIPEA). Intermediate **1** was deprotected with 4M HCl in dioxane to obtain the free amine **2**, which was reacted with selected carboxylic acids through a HATU-supported amide coupling to give the corresponding acyl dipeptides **3a-i**. Compounds **3a**, **3b**, and **3i** were saponified with NaOH in MeOH to receive the carboxylic acids **4a**, **b**, and **i**, which were subjected to HATU-assisted coupling reactions, leading to the pyridinyl esters **5b** and **5i**, as well as to the peptide nitriles **6** and **7**.

Further envisaged compounds, *i.e.*, **9** and **11**-**14**, were synthesized as shown in Scheme 2. To prepare the aldehydes **9a-c**, the ethyl esters **3a-c** were reduced with NaBH_4 in MeOH/THF to give the corresponding alcohols **8a–c**. These were oxidized with Dess-Martin periodinane, and the desired aldehydes **9a-c** were obtained. Compound **9a** was converted through a condensation-dehydration sequence with hydroxylamine hydrochloride and TiCl_4 in pyridine to give the nitrile **11a**. Two aldehydes, **9a–b**, were employed as substrates for HWE (Horner-Wadsworth-Emmons) reactions, yielding the corresponding vinyl sulfones **12a–b** or β-substituted acrylamides **13a-b**. From the acrylamides, acrylonitriles **14a–b** were prepared by dehydration with cyanuric chloride. Furthermore, esters **3b-h** were converted with methanolic ammonia to primary carboxamides **10b–h**, which were then dehydrated to **11b-h**, representing the majority of acylated dipeptide nitriles.
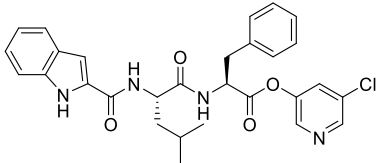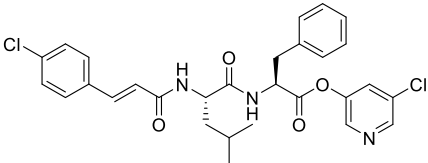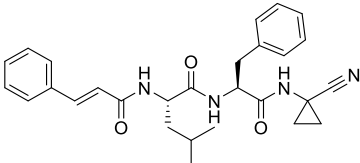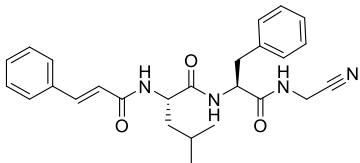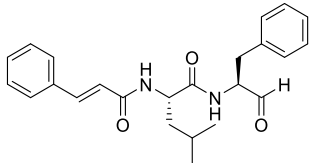
2.3. Evaluation of protease inhibition and structure-activity relationships.

According to previously described procedures,[35-37] the cathepsin inhibition assays were performed with an appropriate chromogenic peptide substrate. We used Z-Phe-Arg-pNA and Z-Arg-Arg-pNA for human CatL and human CatB, respectively. To monitor the activity of human CatS, Bz-Phe-Val-Arg-pNA was established as a chromogenic substrate and its K_m value was determined to be 61.9 μM. All final compounds were tested at a concentration of 10 μM (Table 1). In cases of more than 30% protease inhibition over 60 min, the compounds were investigated at five different concentrations; the slopes of the progress curves were plotted *versus* inhibitor concentrations, and K_i values were obtained by non-linear regression. A SARS-CoV-2 M^pro activity assay with a recently developed fluorogenic substrate (Boc-Abu-Tle-Leu-Gln-AMC) was employed,[10,38] compounds were screened at a concentration of 10 μM, and for selected active representatives, K_i values were determined (Table 1).

Scheme 2. Synthesis of Compounds 9a–c, 11a–h, 12a–b, 13a-b, and 14a–b[a]

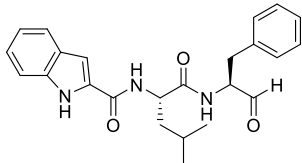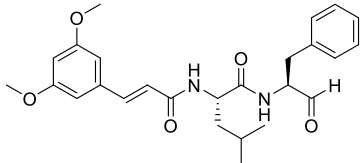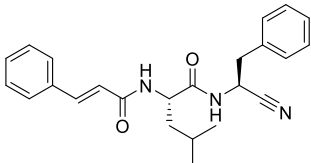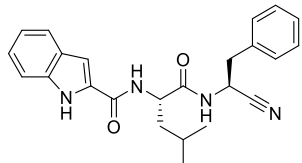
- **a** R = cinnamoyl
- **b** R = 1*H*-indole-2-carbonyl
- **c** R = 3-(3,5-dimethoxyphenyl)acryloyl
- **d** R = 2-(4-chlorophenoxy)acetyl
- **e** R = 2-(2,4-dichlorophenoxy)acetyl
- **f** R = 2-(3-(dimethylamino)phenoxy)acetyl
- **g** R = chromane-2-carbonyl
- **h** R = 5-phenylfuran-2-carbonyl

[a]Reagents and conditions: (i) 7M NH_3 in MeOH, 25 °C, 78-100%; (ii) cyanuric chloride, DMF (dry), 0→25 °C, 42-87%; (iii) NaBH_4, MeOH, THF, 0 °C, 79-100%; (iv) Dess–Martin periodinane, CH_2Cl_2 (dry), 0 °C, 20-95%; (v) a. hydroxylamine × HCl, TiCl_4, pyridine (dry); b. 5% aq. NaHSO_4, 22%; (vi) diethyl ((phenylsulfonyl)methyl)phosphonate, lithium bis(trimethylsilyl)amide in THF, THF (dry), -78 °C, 39-71%; (vii) diethyl (2-amino-2-oxoethyl)phosphonate, LiCl, 1,8-diazabicyclo[5.4.0]undec-7-ene, MeCN (dry)/CHCl_3 (dry), 47-48%.

4

Table 1. Structures and Biological Activities of Investigated Compounds

Compound	Cathepsin L K_i (μM)^{a,b}	Cathepsin B K_i (μM)^{a,c}	Cathepsin S K_i (μM)^{a,d}	SARS-CoV-2 M^{pro} K_i (μM)^e	SARS-CoV-2 (Calu-3-cells) EC$_{50}$ (μM)^f
5b	1.19 ± 0.03	22.1 ± 0.9	0.0270 ± 0.0032	3.06 ± 0.19	n.d.^{g}
5i	n.i.^{h}	n.i.^{h}	5.23 ± 0.47	1.43 ± 0.10	n.d.
6	1.57 ± 0.09	n.i.	2.45 ± 0.16	>5^i	n.d.
7	0.596 ± 0.040	63.8 ± 17.8	0.864 ± 0.036	>5	n.d.
9a	0.00267 ± 0.00019	0.0894 ± 0.0030	0.000455 ± 0.000028	>5	0.0610
9b	0.00176 ± 0.00011	0.136 ± 0.008	0.000512 ± 0.000031	1.41 ± 0.19	0.173
9c	0.0150 ± 0.0006	0.218 ± 0.005	0.00129 ± 0.00009	3.41 ± 0.22	2.72
11a	0.725 ± 0.029	n.i.	0.0478 ± 0.0027	>5	n.d.
11b	1.25 ± 0.09	18.4 ± 1.0	0.0771 ± 0.0057	>5	0.729

5

	Structure					
11c		n.i.	n.i.	0.848 ± 0.070	>5	n.d.
11d		0.870 ± 0.097	n.i.	0.0767 ± 0.0122	>5	0.372
11e		0.111 ± 0.007	n.i.	0.103 ± 0.011	>5	0.0351
11f		0.474 ± 0.054	n.i.	0.169 ± 0.010	>5	n.d.
11g		0.00956 ± 0.00036	n.i.	0.0169 ± 0.0017	>5	2.70
11h		1.92 ± 0.22	n.i.	0.0890 ± 0.0110	>5	n.d.
12a		0.625 ± 0.064	9.49 ± 0.48	0.00496 ± 0.00029	>5	n.d.
12b		0.243 ± 0.014	n.i.	0.00962 ± 0.00070	>5	>10
13a		n.i.	n.i.	0.367 ± 0.027	>5	n.d.
13b		3.16 ± 0.15	n.i.	0.816 ± 0.102	>5	n.d.

6

14a		1.40 ± 0.13	12.4 ± 1.4	0.118 ± 0.005	>5	n.d.
14b		4.06 ± 0.28	n.i.	0.671 ± 0.072	>5	n.d.

[a] Reactions were followed at 37 °C for 60 min. The formation of the product was monitored at 405 nm. The progress curves were analyzed by linear regression. K_i values were obtained from duplicate measurements with five different inhibitor concentrations and analyzed by non-linear regression using the equation $v = v_0/(1 + [I]/(K_i \times (1 + [S]/K_m))$, where v and v_0 are the product formation rates in the presence and absence of inhibitor, [S] is the substrate concentration, and K_m is the Michaelis constant. The standard errors (SE) refer to the non-linear regression.

[b] The final substrate concentration of the chromogenic substrate Z-Phe-Arg-pNA was 100 μM.

[c] The final substrate concentration of the chromogenic substrate Z-Arg-Arg-pNA was 500 μM.

[d] The final substrate concentration of the chromogenic substrate Bz-Phe-Val-Arg-pNA was 70 μM.

[e] The final substrate concentration of the fluorogenic substrate Boc-Abu-Tle-Leu-Gln-AMC was 50 μM and the formation of the product was monitored with excitation and emission at wavelengths of 360 nm and 460 nm, respectively. Reactions were followed at 37 °C for 60 min. The progress curves were analyzed by linear regression. IC50 values were obtained from duplicate measurements with five different inhibitor concentrations and analyzed by non-linear regression using the equation $v = v_0/(1 + [I]/(K_i \times (1 + [S]/K_m))$, where v and v_0 are the product formation rates in the presence and absence of inhibitor, [S] is the substrate concentration, and K_m is the Michaelis constant, being 48 μM. The standard errors (SE) refer to the non-linear regression.

[f] EC50 values of inhibitors in Calu-3 cells. Lung-derived human Calu-3 cells were incubated with 10-fold serial dilutions (10−0.001 μM) of each inhibitor or DMSO (solvent control) for 1 h, followed by infection with SARS-CoV-2 at a multiplicity of infection (MOI) of 0.01.

[g] n.d., Not determined.

[h] n.i., No inhibition. The residual cathepsin activity in the presence of 10 μM of the test compound was higher than 70%.

[i] A K_i value of >5 μM referred to the residual activity of M^{pro} in the presence of 10 μM of the test compound being higher than 70%.

The scaffold of all designed inhibitors was composed of a Leu-Phe dipeptide portion. In most cases, leucine was placed at P2 and phenylalanine at P1. In contrast, in compounds **6** and **7**, a nitrile moiety derived from 1-aminocyclopropane-1-carboxylic acid (ACC) and glycine, respectively, was added C-terminally from the Leu-Phe portion, shifting it to the P3-P2 position. A variety of well-known warheads was incorporated, most of which were susceptible to the nucleophilic addition of the active site cysteine residues of the proteases.[39] We equipped compounds **6**, **7**, and **11a**-**h** with a nitrile warhead, **9a**-**c** with an aldehyde, and **12a**-**b**, **13a**-**b**, and **14a**-**b** with a Michael acceptor. The extended α,β-unsaturated moiety in **12-14** might be engaged in interacting with the S1' pocket of the target cysteine proteases. Peptides **5b** and **5i** possess a cleavable warhead structure. Their design was geared to the structure of 5-halopyridin-3-yl 1H-indole-carboxylates,[10] whose indole unit was replaced by the peptide core present in **5b** and **5i**. Mainly, two N-terminal groups were introduced, i.e., the 1H-indole-2-carbonyl and the cinnamoyl group. The indole capping group has already been incorporated into efficient peptidic inhibitors of the main protease of coronaviruses.[38,40]

Initially, we paid attention to the inhibition of our primary targets, i.e., CatL and SARS-CoV-2 M^{pro}. In compound **5b**, the Leu-Phe dipeptide portion was combined with the indole capping group and equipped with a 5-chloropyridin-3-yl ester at the C-terminus. Inhibition of both target proteases was observed, however, with K_i values only in the single-digit micromolar range. Both tripeptide nitriles **6** and **7** were active against CatL, but failed to inhibit M^{pro}.

Peptide aldehydes **9a**–**c** were identified as extremely potent CatL inhibitors (Figure 4). The representatives with the preselected cinnamoyl and 1H-indole-2-carbonyl capping groups, i.e., **9a** and **9b**, exhibited K_i values of 2.67 nM and 1.76 nM. The introduction of two methoxy groups at the cinnamoyl moiety slightly reduced CatL inhibitory activity (**9c** vs. **9a**). Aside from the electrophilic reactivity of the warhead, the other structural components contribute to the binding affinity of the extraordinarily potent CatL inhibitors **9a** and **9b**. The side chains of phenylalanine and leucine are expected to occupy the S1 and S2 specificity pockets, respectively, and the N-terminal capping group is thought to be accommodated in the S3 binding site. Peptide aldehyde **9b** also showed inhibition of SARS-CoV-2 M^{pro}, albeit in the micromolar range (Figure 4).

7
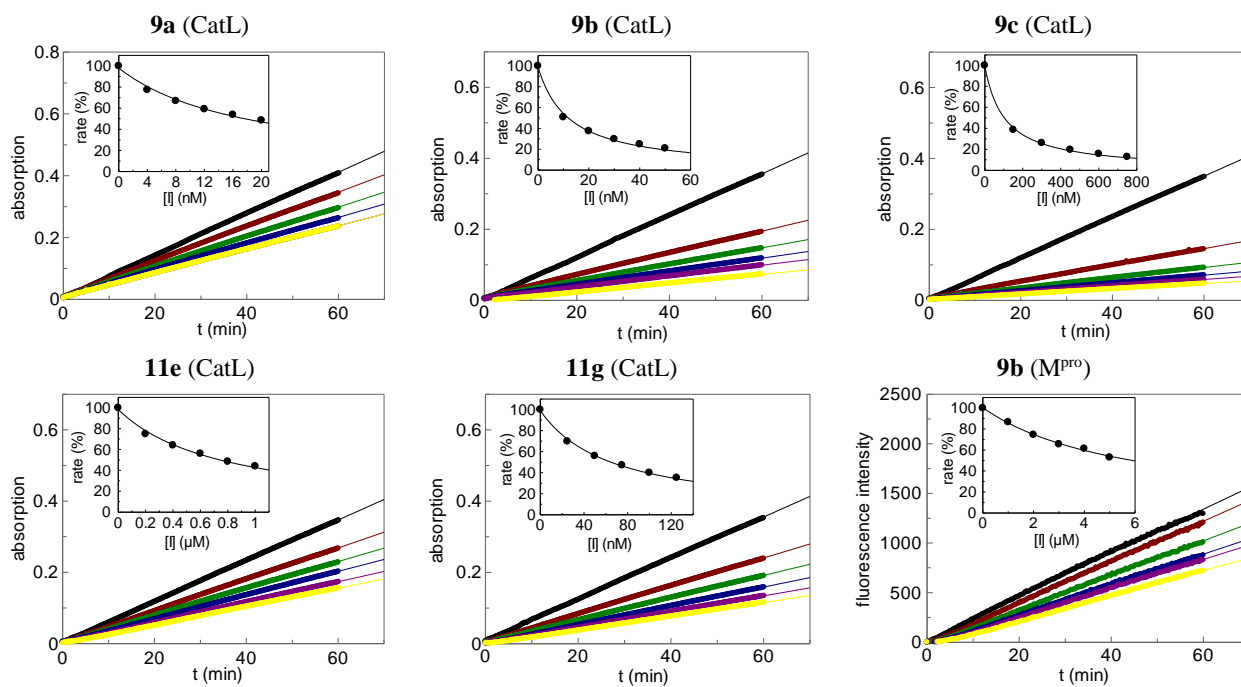
Figure 4. Concentration-dependent inhibition of human CatL by inhibitors **9a** (K_i = 0.00267 μM), **9b** (K_i = 0.00176 μM), **9c** (K_i = 0.0150 μM), **11e** (K_i = 0.111 μM), and **11g** (K_i = 0.00956 μM), as well as SARS-CoV-2 M[pro] inhibition by compound **9b** (K_i = 1.41 μM).

The nitrile group was introduced in place of the aldehyde in the following set of compounds (**11a-h**) with various P3 moieties. Since the Leu-Phe portion was kept constant, these compounds allowed for an optimization of the P3 moiety. Compound **11a** with the unsubstituted cinnamoyl group demonstrated good CatL inhibition in contrast to its 3,5-dimethoxy derivative **11c**, likely because of an unfavorable steric interaction. The indole derivative **11b** was a somewhat weaker inhibitor than **11a**. The three phenoxyacetyl derivatives **11d-f** demonstrated effective CatL inhibition with K_i values between 111 nM and 870 nM. Fascinatingly, the cyclic form of the phenoxyacetyl derivative **11g** showed excellent CatL inhibition with a K_i value of 9.56 nM (Figure 4), indicating that rigidization accounted for a favorable binding mode of **11g**. None of the peptide nitriles inhibited SARS-CoV-2 M[pro].

As an alternative to nitriles and aldehydes, compounds with Michael acceptor moieties were investigated. Each of the three pairs consisted of one compound with the cinnamoyl group and the other with the 1*H*-indole-2-carbonyl capping group. Both vinyl sulfones exhibited significant CatL inhibition (**12a**, K_i = 625 nM; **12b**, K_i = 243 nM). The Michael acceptor moiety present in **12a** and **12b** turned out to be advantageous in comparison with both the acrylamide (**13a-b**) and acrylonitrile (**14a**–**b**) warhead structures. The impact of the N-terminal capping group on the CatL-inhibitory potency was difficult to determine. In some cases (**9a** *vs*. **9b**, **12a** *vs*. **12b**, **13a** *vs*. **13b**), the corresponding 1*H*-indole-2-carbonyl analog was more potent; in other cases (**11a** *vs*. **11b**, **14a** *vs*. **14b**), the cinnamoyl counterpart. Overall, SARs of the dipeptide derivatives clearly indicated that the nature of the warhead group played a significant role in inhibiting the target CatL. In particular, it was discovered that the best warhead was the highly electrophilic aldehyde moiety. The rank order of potency for warhead groups

in our CatL inhibitors was as follows: CHO > CN ≈ vinyl sulfone > pyridyl ester ≈ acrylonitrile ≈ acrylamide.

Next, the CatB and S inhibitory activities of the compounds were inspected. By trend, a less pronounced inhibition of CatB was observed in comparison to CatL (Table 1). On the contrary, the compounds were highly potent inhibitors of CatS. This finding was expected because leucine is known as a preferred P2 amino acid in CatS substrates and the Leu-Phe dipeptide as an advantageous P2-P1 pattern in peptidomimetic CatS inhibitors.[41-43] The majority of compounds did not show CatB inhibition, and **5b**, **11b**, **12a**, and **14a** exhibited K_i values in the range of 9 μM to 22 μM. These four compounds inhibited CatS with K_i values between 5 nM and 118 nM. Three compounds were potent CatB inhibitors, *i.e.*, **9a**, **9b**, and **9c**, with K_i values lower than 220 nM. Even these three peptide aldehydes had a clear preference for CatL over CatB, with K_i values being lower by one order of magnitude (Table 1). However, **9a**, **9b**, and **9c** were identified as sub-nanomolar or single-digit nanomolar CatS inhibitors (Table 1).

To revisit M[pro] inhibitory activity, we did not identify an inhibitor that was active in the nanomolar range. This finding was in sharp contrast to the outstanding activity against cathepsins that we observed for certain representatives. Only the aldehydes **9b** (Figure 4) and **9c** displayed moderate M[pro] inhibitory activities that were accompanied by their extremely strong potency against cathepsins. Considering the capability of cathepsins to proteolytically activate coronaviral spike proteins via the endosomal pathway,[19,23,26] the most promising compounds were subjected to an investigation of their antiviral activity.

8

2.4. Cytotoxicity and antiviral activity against SARS-CoV-2. Before evaluating their antiviral activity in Calu-3 cells, a subseries of compounds (**9a–c**, **11b,d,e,g**, **12b**) was investigated for potential cytotoxicity on Calu-3 cells at a high concentration of 10 μM. None of the compounds exhibited cytotoxicity at the given concentration. Calu-3 cells, which were infected with SARS-CoV-2, were used to test the antiviral activity of the selected compounds (**9a-c**, **11b,d,e,g**, **12b**). Figure 5 illustrates the activity against SARS-CoV-2, Pango lineage B.1.513. We employed molnupiravir, a recognized and authorized SARS-CoV-2 inhibitor, as a positive control.[44] The cells were incubated 1 hour before infection with SARS-CoV-2 at a multiplicity of infection (MOI) of 0.01 and 24 hours post-infection (*p.i.*) with 10-fold serial dilutions (10-0.001 μM) of each inhibitor. Viral titers of Calu-3 cell culture supernatants were determined by titration on Vero E6 cells 24 h *p.i.* and are expressed as plaque-forming units (PFU) per milliliter. From these data, EC_{50} values were calculated (Table 1).

The three peptide aldehydes (**9a**, **9b**, and **9c**) exhibited antiviral activity. Strikingly, the two potent CatL, B, and S inhibitors **9a** and **9b** possessed a more pronounced efficacy as antiviral agents with submicromolar EC_{50} values compared to **9c**, which had moderate inhibition. These data pointed to a connection between cathepsin inhibiting and antiviral properties.

The aldehyde inhibitor **9b** with a P3-indole capping group also showed moderate inhibition of M^{pro}. This prompted us to focus on analogs of **9b** with an altered warhead structure, and the nitrile **11b** as well as the Michael acceptor **12b** were also evaluated with respect to their antiviral activity. Although **11b** and **12b** were found to be more than 100-fold weaker CatL inhibitors than **9b**, one of the analogs, *i.e.*, **11b**, exhibited

antiviral activity. This result was unexpected and indicated that potent *in vitro* activity against CatL was not a prerequisite for activity in the cellular antiviral test system. A correlation between the CatL and antiviral data for the other three nitrile inhibitors **11d,e,g** was also not evident, since in the case of **11g**, the highly efficient CatL inhibition (K_i = 9.56 nM) was not accompanied by strong effects against viral infection, whereas the rather weak CatL inhibitor **11e** was potent in the antiviral assay exhibiting an EC_{50} value of 35.1 nM. This compound might act through interference with another biological target, which must be investigated in future studies.

2.5. Molecular modeling of potent inhibitors with cathepsin L. Using molecular modeling, we proposed a binding mode for **9b** and **11g** as representatives of the peptide aldehydes and peptide nitriles investigated in this study. For this purpose, covalent docking was applied to generate the inhibitor-protein complex with the initial conformation of the inhibitor, followed by molecular dynamics simulations to corroborate the proposed interactions. We also performed simulations to compare the binding mode of our CatL inhibitors with that of the co-crystallized inhibitor XU3 (PDB ID: 2XU3).[45] Peptide aldehydes form reversible-covalent complexes with cysteine proteases with a tetrahedral geometry of the resulting hemithioacetals with an sp^3 hybridization. Hence, they act as transition state analogs. Peptide nitriles generate a covalent linkage with cysteine proteases adopting a trigonal geometry of the thioimidate moiety possessing an sp^2 hybridization, which rather resembles the acyl enzyme intermediate.[46,47]
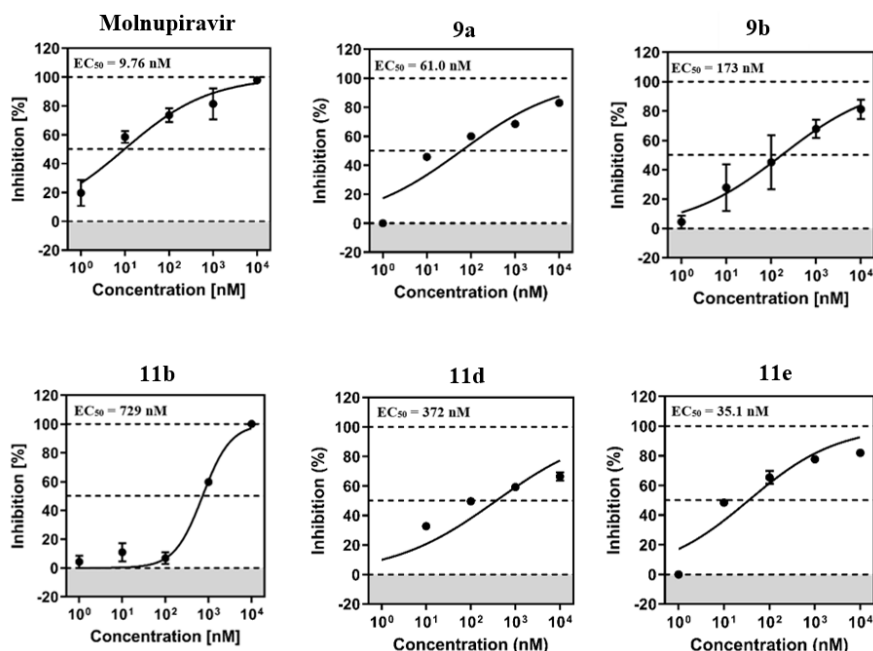
Figure 5. EC_{50} values of cathepsin inhibitors in Calu-3 cells. Lung-derived human Calu-3 cells were incubated with each inhibitor or DMSO (solvent control) for 1 h, followed by infection with SARS-CoV-2. After virus inoculation, cells were further incubated with the respective inhibitors for 24 h. Supernatants were harvested, and viral titers were determined by titration on Vero E6 cells. For normalization, viral titers of DMSO-treated cells were set at 0% inhibition. Means ± SDs from three biological replicates are presented.

9
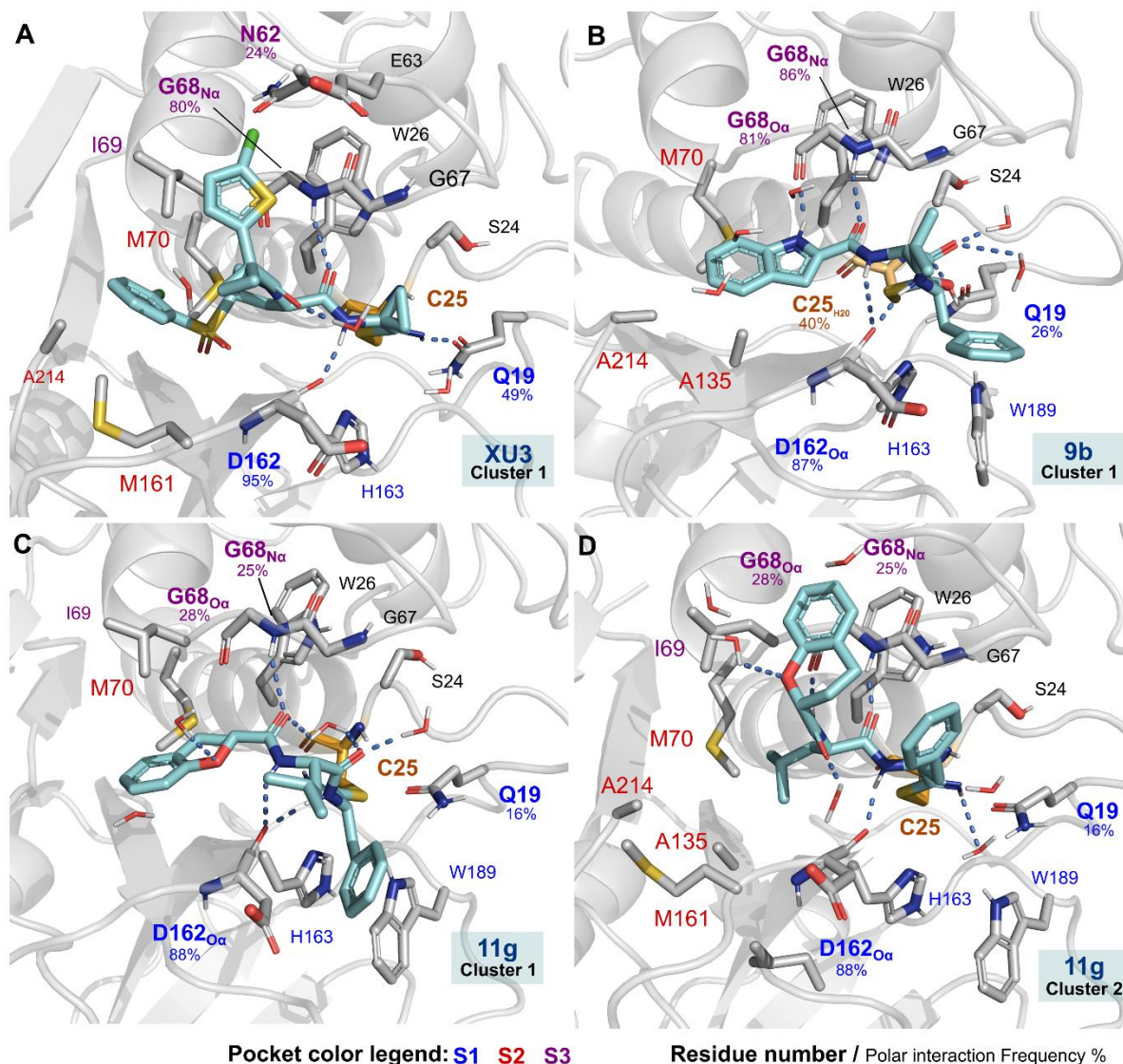
Figure 6. Proposed binding mode for our cathepsin L inhibitors in comparison to the co-crystallized ligand (XU3) from PDB 2XU3. A representative simulation frame was selected by clustering for the simulations of XU3 (A) and **9b** (B), while compound **11g** displayed two relevant clusters (C, D). Amino acids and ligands are depicted as sticks, and their labels are colored according to the described pockets (S1, blue; S2, red; and S3, purple). The frequency values for the protein-ligand polar interactions (H-bond or water-bridge) along the 5 µs (for each ligand) analyzed simulation trajectories are displayed below the labels.

The XU3 inhibitor is a peptide nitrile that forms a covalent thioimidate connection with the active site cysteine of CatL. Simulations of the CatL-XU3 complex (Figure 6A) recapitulated the hydrogen bond interactions of the inhibitor with the backbone CO of Asp162 (in the S1 subsite, 95% of the analyzed trajectory) and the backbone NH of Gly68 (in the S3 subsite, with a frequency of ~80%), as well as multiple hydrophobic contacts with the S2 and S3 pockets.[45] The new inhibitors **9b** and **11g** were also proposed to covalently bind to the catalytic Cys25 residue (Figure 6B-D) in the S1 pocket. The hemithioacetal and thioimidate adducts, respectively, were stabilized by the oxyanion hole of the protease. The inhibitors also formed hydrogen bonds to the backbone carbonyl oxygen of Asp162 (>85% of the analyzed trajectory). Figure 5B illustrates the major representative cluster of **9b**-CatL

complexes. The indole-2-carbonyl moiety of **9b** was engaged in hydrogen bonding to both the CO and NH moiety of Gly68 (~80% of the analyzed trajectory). Additional hydrogen bond interactions are predicted to take place between the two NH groups of the ligand and the Asp162 backbone CO (>85%). We hypothesize that this binding mode enables **9b** to be in a position that allows the covalent bond to be formed.

Compound **11g** showed an intermittent interaction (cluster 1, Figure 6C) of the chromane carbonyl group with the Gly68 NH (~25%). However, in cluster 2 (Figure 6D), a rotation of the chromane ring led to the occupation of this moiety in the S3 pocket, and leucine at P2 position is oriented towards the S2 subsite. In the case of **11g**, the S2 pocket is accommodated by a much smaller moiety in comparison with XU3 (Figures 6A, D). Both inhibitors share the nitrile warhead, but XU3 is a less potent CatL inhibitor (IC$_{50}$ = 160 nM).[45]

10

2.6. Glutathione stability. To determine the innate reactivity of inhibitors with electrophilic warheads towards thiols under physiological conditions, we tested the stability of three selected compounds, *i.e.,* the peptide nitriles **11b** and **11e** and the peptide aldehyde **9b**, in the presence of excess glutathione (GSH) as a physiological nucleophile (Figure S1). These investigations demonstrated the low inherent reactivity of the inhibitors, which were stable under assay conditions (5 mM GSH, pH 7.4). Hence, the specific reactivity towards cathepsins is caused by the formation of the inhibitor-target complex and supported by tailored non-covalent interactions.

2.7. Pharmacokinetic *in vitro* studies. Metabolic stability is the basic prerequisite for the start of further *in vivo* studies. Initially, we investigated the metabolic stability of compound **11b** in mouse liver microsomes (MLMs) and human liver microsomes (HLMs) *in vitro* (Figure S2). It was observed that **11b** was metabolized to an extent of only 23% by HLMs after 120 min (Table S3). Although **11b** underwent substantially higher metabolization in MLMs, nearly 50% of the compound was still retained. We next assessed the metabolic stability of a compound from our study that is distinguished by its antiviral activity, *i.e.*, **11e**. In contrast to **11b**, compound **11e** was entirely stable in MLMs and HLMs, with half-lives ($t_{1/2}$) of more than 60 min each. In addition, the intrinsic clearance of **11e** was determined in the mouse model and, gratifyingly, was below 23 μL/min/mg, indicating that the compound is stable. Encouraged by these results, we assessed plasma stability as well as plasma protein binding (PPB) in the next step. Again, **11e** was very stable in mouse and human plasma, as no degradation was observed up to 240 min. With respect to PPB, **11e** exhibited a high protein binding in mouse and human of about 99%. In summary, **11e** showed favorable pharmacokinetic properties for further preclinical development.

2.8. Conclusions. In summary, we developed a new class of small-molecule peptidomimetics based on the virtual screening of a kinase inhibitor collection for their inhibition of human cathepsins, the host cysteine proteases involved in the pathogenesis of SARS-CoV-2. The molecular design included three fragments, out of which the N-terminal capping group and the C-terminal warhead were diversified, and the central Leu-Phe dipeptide fragment was maintained. This approach resulted in a variety of highly effective CatL and CatS aldehyde-type inhibitors, including those with low nanomolar to subnanomolar K_i values, *i.e.*, **9a**–**c**. Compounds with the nitrile warhead (**11a** and **11d**-**g**) have also been identified as dual CatL and S inhibitors. Most inhibitors were selective for CatL and S

over human CatB. The cellular role of human CatS for viral infection is much less defined than that of CatL.[27] However, recent studies underlined that CatS contributes to acute lung injury and may represent a novel therapeutic target to combat respiratory diseases. Hence, CatS inhibition may be a desirable feature of anti-SARS-CoV-2 drugs.[48] In general, cathepsin inhibition was not accompanied by similarly pronounced M[pro] inhibition. When subjecting selected compounds to an evaluation of their antiviral properties, we identified certain peptidomimetics that effectively prevented SARS-CoV-2 infection in Calu-3 cells. The peptide nitrile **11e** showed high antiviral activity with an EC_{50} value of 35.1 nM, displayed no cytotoxicity, and exhibited high metabolic stability, making it a suitable drug for further preclinical development.

3. EXPERIMENTAL SECTION

3.1. Chemistry. *General information.* All commercially available starting materials, reagents, and (anhyd.) solvents were used without further purification. Reaction controls were performed by thin-layer chromatography (TLC) on Macherey-Nagel precoated 60 F254 silica plates. Spots were visualized either by ultraviolet (UV) light (254 nm/365 nm) or staining solutions. Flash column chromatography was carried out using Grace Davison Davisil LC60A (20–45 μm) or Merck Geduran Si60 (mesh 63–200 μm) with an Interchim PuriFlash 430 automated flash chromatography system. NMR spectra were recorded on a Bruker Avance 400 MHz spectrometer at ambient temperature. Chemical shifts (δ) are reported in parts per million (ppm) relative to the internal control tetramethylsilane (TMS) and the spectra were calibrated against the residual solvent peak of the used deuterated solvent. Coupling constants (*J*) are expressed in Hertz (Hz). Purities of final compounds were determined by RP-HPLC using an Agilent 1100 Series LC with a Phenomenex Luna C8 analytical column (150 × 4.6 mm, 5 μm) and detected by a UV DAD detector at 254 nm wavelength. Elution was carried out with the following gradient: (A = 0.01 M KH_2PO_4, pH 2.30, B = MeOH) 40% B to 85% B in 8 min, 85% B for 5 min, 85% to 40% B in 1 min, 40% B for 2 min, stop time 16 min, flow 1.5 mL/min. Standard mass spectra were obtained from an Advion expression compact mass spectrometer (electron spray ionization, ESI) with a TLC plate reader system (using the following settings: ESI voltage 3.50 kV, capillary voltage 187 V, source voltage 44 V, capillary temperature 250 °C, desolvation gas temperature 250 °C, gas flow 5 L/min). All final compounds are ≥ 95% pure by HPLC.

Table 2. Pharmacokinetic properties of 11e in mouse and human plasma

$t_{1/2}$ (min) MLMs	$t_{1/2}$ (min) HLMs	Cl_{int} (μL/min/mg) mouse	$t_{1/2}$ (min) mouse plasma	$t_{1/2}$ (min) human plasma	PPB (%) mouse[a]	PPB (%) human[a]
> 60	> 60	< 23	> 240	> 240	99.2 ± 0.5	99.5 ± 0.4

[a]Means ± SDs from 3 replicates are presented.

11
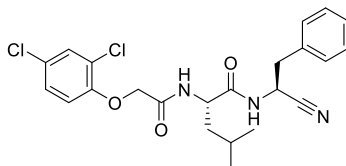
General procedure A for the synthesis of carboxamides. HATU (2.4 mmol, 1.2 equiv.) was added sequentially at 0 °C to the solution of the acid (2 mmol, 1 equiv.) in DMF (5 mL). The solution was kept at 0 °C for 30 min. After that, DIPEA (6 mmol, 3 equiv.) and the amine (2 mmol, 1 equiv.) were slowly added. The mixture was stirred at 0 °C for 1 h and at 25 °C for 12 h. The reaction was quenched by adding water and extracted with EtOAc (3 × 15 mL). The combined organic phases were washed with sat. NH_4Cl solution (2 × 50 mL), sat. $NaHCO_3$ solution (2 × 50 mL) and brine (2 × 50 mL). The organic layer was dried over Na_2SO_4 and concentrated under reduced pressure to the dryness.

General procedure B for the saponification of esters. To a solution of the ester (1 mmol) in MeOH (20 mL) was added 10 mL of an aq. NaOH solution (2.0 M). The reaction was stirred at room temperature, and the progress of the reaction was monitored by TLC. After full conversion (2-3 h), the volume was reduced *in vacuo*, and the mixture was cooled, gently acidified with 2 N HCl, and extracted with EtOAc (3 × 15 mL). The combined organic phases were dried over Na_2SO_4, filtered, and removed under reduced pressure. The product was used for the next step without further purification.

General procedure C for the Boc deprotection. The *N*-Boc-protected amine (1.5 mmol, 1 equiv.) was dissolved in CH_2Cl_2 (3 mL), and 4 N HCl in dioxane (11.5 mmol, 10 equiv.) was added at 0 °C. The mixture was stirred for 3 h at 0 °C. The reaction was concentrated under reduced pressure to give the HCl salt, which was dissolved in aq. 0.05 M NaOH and extracted with EtOAc (3 × 15 mL). The combined organic layers were dried over Na_2SO_4, filtered, and concentrated under reduced pressure. The product was used for the next step without further purification.

General procedure D for the ammonolysis of esters. A methanolic solution of ammonia (10 mL, 7 M) was added to the ethyl ester (1 mmol), and it was stirred at 25 °C for 48 h. After full consumption, the mixture was concentrated under reduced pressure to get the corresponding primary carboxamide.

General procedure E for the dehydration of primary amides. Cyanuric chloride (1 mmol, 1 equiv.) was dissolved in ice cooled DMF (dry) and stirred for 10 min before the primary amide (1 mmol, 1 equiv.) was added dropwise as a solution or suspension in DMF (dry). After addition, the reaction was allowed to reach 25 °C and was stirred overnight. The reaction was quenched with sat. $NaHCO_3$ solution and extracted with EtOAc (4 × 15 mL). The combined organic phases were washed with brine, dried over Na_2SO_4, filtered, and concentrated under reduced pressure to afford the nitrile.

General procedure F for the reduction of esters to alcohols. To a solution of the ester (0.5 mmol, 1 equiv.) in THF (dry), $NaBH_4$ (3 mmol, 6 equiv.) was added portion-wise at 0 °C. MeOH (2 mL) was added dropwise, and then the reaction mixture was stirred at room temperature for 3 h. The completion of the reaction was confirmed by TLC, and it was quenched with sat. NH_4Cl solution (20 mL). The mixture was extracted with EtOAc (3 × 50 mL) and the organic layers were washed with sat. NH_4Cl solution (2 × 20 mL) and brine (2 × 50 mL). The organic phase was dried over Na_2SO_4, concentrated under reduced pressure, and the residue purified by flash column chromatography to afford the alcohol.

General procedure G for the Dess-Martin oxidation of alcohols to aldehydes. To a solution of the alcohol (0.5 mmol,

1 equiv.) in CH_2Cl_2, Dess-Martin periodinane (0.6 mmol, 1.2 equiv.) was added slowly at 0 °C. The reaction mixture was stirred at 0 °C until the reaction was completed, which was monitored by TLC. It was filtered and washed with sat. $Na_2S_2O_3$ solution (2 × 20 mL), sat. $NaHCO_3$ solution (2 × 20 mL) and brine (1 × 20 mL). The organic phase was dried over Na_2SO_4 and concentrated under reduced pressure to dryness. The residue was purified by flash column chromatography to afford the aldehyde.

General procedure H for the HWE reaction to obtain vinyl sulfones. Diethyl ((phenylsulfonyl)methyl)phosphonate (0.5 mmol, 1 equiv.) was dissolved in THF (dry, 5 mL) under an argon atmosphere. The solution was cooled to -78 °C, and a 1 M solution of lithium bis(trimethylsilyl)amide (0.6 mmol, 1.2 equiv.) in THF was added dropwise. The mixture was stirred for an additional 30 min at the same temperature before the aldehyde (0.5 mmol, 1 equiv.) was added. The reaction temperature was kept at -78 °C for 2 h before it was slowly heated up to 0 °C. Water (15 mL) was added, and the phases were separated. The aq. layer was extracted with EtOAc (3 × 15 mL). The organic layers were combined and washed with sat. NH_4Cl solution (2 × 15 mL), sat. $NaHCO_3$ solution (2 × 15 mL), and brine (1 × 15 mL). The solvent was removed under reduced pressure after drying over Na_2SO_4. The resulting crude product was purified by flash column chromatography to afford the vinyl sulfone. The compounds were isolated as a mixture of E/Z isomers, resulting in NMR spectra of high complexity.

General procedure I for the HWE reaction to obtain acrylamides. Diethyl (2-amino-2-oxoethyl)phosphonate (0.75 mmol, 1.5 equiv.) and 1,8-diazabicyclo[5.4.0]undec-7-ene (0.75 mmol, 1.5 equiv.) were added to a suspension of LiCl (0.75 mmol, 1.5 equiv.) in MeCN (dry, ~ 0.2 M). The mixture was stirred for 10 min at ambient temperature before the aldehyde (0.5 mmol, 1 equiv.) was added as a suspension in chloroform (dry, ~ 0.8 M). The reaction was monitored via TLC and quenched after complete conversion with sat. NH4Cl solution. Water (15 mL) was added, and the phases were separated. The aq. layer was extracted with EtOAc (3 × 15 mL), and the combined organic layers were washed with sat. NH_4Cl solution (2 × 15 mL), sat. $NaHCO_3$ solution (2 × 15 mL), and brine (1 × 15 mL). The solvent was removed under reduced pressure after drying over Na_2SO_4. The resulting crude product was purified by flash column chromatography. The compounds were isolated as a mixture of E/Z isomers, resulting in NMR spectra of high complexity.

Ethyl (tert-butoxycarbonyl)-L-leucyl-L-phenylalaninate (1). This product was obtained by reacting L-phenylalanine ethyl ester hydrochloride (458 mg, 2 mmol) with N-Boc-L-leucine monohydrate (497 mg, 2 mmol) according to procedure A. Yield: 505 mg (67%) of **1** as a white solid. ^{1}H NMR (400 MHz, CDCl$_3$) δ 7.33 – 7.26 (m, 3H), 7.17 – 7.13 (m, 2H), 6.52 (d, *J* = 7.7 Hz, 1H), 4.95 – 4.75 (m, 2H), 4.18 (q, *J* = 7.1 Hz, 2H), 4.14 – 4.06 (m, 1H), 3.21 – 3.09 (m, 2H), 1.72 – 1.60 (m, 2H), 1.47 (s, 9H), 1.45 – 1.39 (m, 1H), 1.25 (t, *J* = 7.1 Hz, 3H), 0.95 (d, J = 4.3 Hz, 3H), 0.94 (d, J = 4.1 Hz, 3H). ESI-MS [M + Na]$^+$ = 429.4. HPLC t$_R$ = 9.52 min.

Ethyl ʟ-leucyl-L-phenylalaninate (2). This product was obtained from (610 mg, 1.5 mmol) according to procedure C. Yield: 460 mg (100%) of **2** as a white solid. ^{1}H NMR (400 MHz, DMSO-d_6) δ 9.12 (d, *J* = 7.2 Hz, 1H), 8.33 (s, 2H), 7.33 – 7.21 (m, 5H), 4.50 (q, *J* = 7.2 Hz, 1H), 4.06 – 3.98 (m, 2H), 3.84 –

12

3.76 (m, 1H), 3.08 – 2.98 (m, 2H), 1.73 – 1.64 (m, 1H), 1.56 (t, J = 7.1 Hz, 2H), 1.08 (t, J = 7.1 Hz, 3H), 0.90 (d, J = 6.5 Hz, 3H), 0.88 (d, J = 6.5 Hz, 3H). ESI-MS [M + H]$^+$ = 307.3. HPLC t_R = 4.60 min.

Ethyl cinnamoyl-L-leucyl-L-phenylalaninate (3a). This product was obtained by reacting cinnamic acid (240 mg, 2.0 mmol) with **2** (613 mg, 2.0 mmol) according to procedure A. Flash purification with CH$_2$Cl$_2$/MeOH (0 - 4% MeOH). Yield: 767 mg (83%) of **3a** as a white solid. ^{1}H NMR (400 MHz, CDCl$_3$) δ 7.63 (d, J = 15.6 Hz, 1H), 7.53 – 7.47 (m, 2H), 7.38 – 7.34 (m, 3H), 7.25 – 7.20 (m, 2H), 7.20 – 7.16 (m, 1H), 7.16 – 7.10 (m, 2H), 6.78 – 6.68 (m, 1H), 6.41 (d, J = 15.6 Hz, 1H), 6.32 – 6.23 (m, 1H), 4.86 – 4.79 (m, 1H), 4.65 – 4.58 (m, 1H), 4.19 – 4.12 (m, 2H), 3.18 – 3.03 (m, 2H), 1.70 – 1.65 (m, 1H), 1.62 – 1.45 (m, 2H), 1.25 – 1.19 (m, 3H), 0.93 (d, J = 6.5 Hz, 3H), 0.90 (d, J = 6.5 Hz, 3H). ESI-MS [M + Na]$^+$ = 459.3. HPLC t_R = 9.43 min.

Ethyl (1H-indole-2-carbonyl)-L-leucyl-L-phenylalaninate (3b). This product was obtained by reacting 1*H*-indole-2-carboxylic acid (225 mg, 2 mmol) with **2** (613 mg, 2 mmol) according to procedure A. Flash purification with CH$_2$Cl$_2$/MeOH (0 - 4% MeOH). Yield: 525 mg (84%) of **3b** as a light-yellow solid. ^{1}H NMR (400 MHz, CDCl$_3$) δ 9.89 – 9.69 (m, 1H), 7.85 – 7.72 (m, 1H), 7.70 – 7.60 (m, 1H), 7.44 – 7.39 (m, 1H), 7.32 – 7.26 (m, 1H), 7.22 – 7.18 (m, 1H), 7.17 – 7.11 (m, 2H), 7.09 – 6.98 (m, 3H), 6.97 – 6.89 (m, 2H), 5.11 – 4.95 (m, 1H), 4.91 – 4.78 (m, 1H), 4.25 – 4.11 (m, 2H), 3.17 – 3.04 (m, 2H), 1.77 – 1.58 (m, 3H), 1.27 – 1.17 (m, 3H), 0.92 (d, J = 6.4 Hz, 3H), 0.89 (d, J = 6.4 Hz, 3H). ESI-MS [M + Na]$^+$ = 472.4. HPLC t_R = 9.37 min.

Ethyl ((E)-3-(3,5-dimethoxyphenyl)acryloyl)-L-leucyl-L-phenylalaninate (3c). This product was obtained by reacting (*E*)-3-(3,5-dimethoxyphenyl)acrylic acid (416 mg, 2 mmol) with **2** (612 mg, 2 mmol) according to procedure A. Flash purification with CH$_2$Cl$_2$/MeOH (0 - 4% MeOH). Yield: 734 mg (84%) of **3c** as a white solid. ^{1}H NMR (400 MHz, CDCl3) δ 7.57 – 7.51 (m, 1H), 7.26 – 7.17 (m, 3H), 7.15 – 7.10 (m, 2H), 6.78 – 6.68 (m, 1H), 6.66 – 6.62 (m, 2H), 6.49 – 6.46 (m, 1H), 6.40 – 6.34 (m, 1H), 6.32 – 6.17 (m, 1H), 4.86 – 4.79 (m, 1H), 4.65 – 4.57 (m, 1H), 4.20 – 4.11 (m, 2H), 3.83 – 3.77 (m, 6H), 3.19 – 3.03 (m, 2H), 1.72 – 1.47 (m, 3H), 1.25 – 1.20 (m, 3H), 0.92 (d, J = 6.1 Hz, 3H), 0.91 – 0.86 (m, 3H). ESI-MS [M + Na]$^+$ = 519.4, HPLC t_R = 9.51 min.

Ethyl (2-(4-chlorophenoxy)acetyl)-L-leucyl-L-phenylalaninate (3d). This product was obtained by reacting 2-(4-chlorophenoxy)acetic acid (373 mg, 2 mmol) with **2** (612 mg, 2 mmol) according to procedure A. Flash purification with CH$_2$Cl$_2$/MeOH (0 - 4% MeOH). Yield: 690 mg (73%) of **3d** as a white solid. ^{1}H NMR (400 MHz, CDCl$_3$) δ 7.28 – 7.22 (m, 4H), 7.20 – 7.15 (m, 1H), 7.14 – 7.08 (m, 2H), 6.88 – 6.77 (m, 3H), 6.48 (d, J = 7.8 Hz, 1H), 4.85 – 4.79 (m, 1H), 4.55 – 4.48 (m, 1H), 4.47 – 4.34 (m, 2H), 4.21 – 4.14 (m, 2H), 3.15 (dd, J = 13.9, 5.8 Hz, 1H), 3.06 (dd, J = 13.9, 6.5 Hz, 1H), 1.70 – 1.64 (m, 1H), 1.59 – 1.47 (m, 2H), 1.26 – 1.22 (m, 3H), 0.90 (d, J = 6.5 Hz, 3H), 0.88 (d, J = 6.4 Hz, 3H). ESI-MS [M + Na]$^+$ = 497.4. HPLC t_R = 15.38 min.

Ethyl (2-(2,4-dichlorophenoxy)acetyl)-L-leucyl-L-phenylalaninate (3e). This product was obtained by reacting 2,4-dichlorophenoxyacetic acid (311 mg, 2 mmol) with **2** (612 mg, 2 mmol) according to procedure A. Flash purification with CH$_2$Cl$_2$/MeOH (0 - 4% MeOH). Yield: 422 mg (59%) of **3e** as

a white solid. ^{1}H NMR (400 MHz, CDCl$_3$) δ 7.44 – 7.40 (m, 1H), 7.24 – 7.20 (m, 3H), 7.18 – 7.15 (m, 1H), 7.12 – 7.10 (m, 2H), 7.05 – 6.99 (m, 1H), 6.81 (d, J = 8.8 Hz, 1H), 6.51 (d, J = 7.8 Hz, 1H), 4.87 – 4.81 (m, 1H), 4.51 – 4.47 (m, 1H), 4.47 – 4.39 (m, 2H), 4.20 – 4.15 (m, 2H), 3.16 (dd, J = 14.0, 5.8 Hz, 1H), 3.08 (dd, J = 13.9, 6.3 Hz, 1H), 1.73 – 1.68 (m, 1H), 1.63 – 1.55 (m, 2H), 1.24 (t, J = 7.1 Hz, 3H), 0.92 (d, J = 6.4 Hz, 3H), 0.90 (d, J = 6.4 Hz, 3H). ESI-MS [M + Na]$^+$ = 531.4. HPLC t_R = 10.52 min.

Ethyl (2-(3-(dimethylamino)phenoxy)acetyl)-L-leucyl-L-phenylalaninate (3f). This product was obtained by reacting 2-(3-(dimethylamino)phenoxy)acetic acid (392 mg, 2 mmol) with **2** (613 mg, 2 mmol) according to procedure A. Flash purification with petroleum ether/EtOAc (0 - 50% EtOAc). Yield: 528 mg (55%) of **3f** as white solid. ^{1}H NMR (400 MHz, CDCl$_3$) δ 7.26 – 7.23 (m, 2H), 7.21 – 7.16 (m, 1H), 7.16 – 7.08 (m, 3H), 6.83 (d, J = 8.4 Hz, 1H), 6.48 (d, J = 7.8 Hz, 1H), 6.43 – 6.39 (m, 1H), 6.29 – 6.22 (m, 2H), 4.85 – 4.78 (m, 1H), 4.53 – 4.38 (m, 3H), 4.21 – 4.14 (m, 2H), 3.15 (dd, J = 13.9, 5.8 Hz, 1H), 3.04 (dd, J = 13.9, 6.6 Hz, 1H), 2.95 (s, 6H), 1.71 – 1.64 (m, 1H), 1.58 – 1.49 (m, 2H), 1.24 (t, J = 7.1 Hz, 3H), 0.89 (d, J = 6.1 Hz, 3H), 0.88 (d, J = 6.0 Hz, 3H). ESI-MS [M + Na]$^+$ = 506.4. HPLC t_R = 9.13 min.

Ethyl ((R,S)-chromane-2-carbonyl)-L-leucyl-L-phenylalaninate (3g). This product was obtained by reacting (*R*,*S*)-chromane-2-carboxylic acid (249 mg, 2 mmol) with **2** (613 mg, 2 mmol) according to procedure A. Flash purification with petroleum ether/EtOAc (0 - 50% EtOAc). Yield: 594 mg (90%) of **3g** as a white solid. ^{1}H NMR (400 MHz, CDCl$_3$) δ 7.23 – 7.11 (m, 3H), 7.10 – 7.04 (m, 2H), 7.00 (d, J = 7.5 Hz, 2H), 6.87 – 6.75 (m, 3H), 6.51 – 6.29 (m, 1H), 4.79 – 4.68 (m, 1H), 4.46 – 4.35 (m, 2H), 4.13 – 4.04 (m, 2H), 3.14 – 2.92 (m, 2H), 2.85 – 2.75 (m, 1H), 2.73 – 2.64 (m, 1H), 2.35 – 2.26 (m, 1H), 1.99 – 1.77 (m, 1H), 1.61 – 1.49 (m, 2H), 1.21 – 1.13 (m, 4H), 0.90 – 0.84 (m, 3H), 0.78 – 0.73 (m, 3H). ESI-MS [M + Na]$^+$ = 489.3. HPLC t_R = 9.74 min.

Ethyl (5-phenylfuran-2-carbonyl)-L-leucyl-L-phenylalaninate (3h). This product was obtained by reacting 5-phenylfuran-2-carboxylic acid (264 mg, 2 mmol) with **2** (612 mg, 2 mmol) according to procedure A. Flash purification with petroleum ether/EtOAc (0 - 50% EtOAc). Yield: 597 mg (89%) of 3h as a white solid. ^{1}H NMR (400 MHz, CDCl$_3$) δ 7.74 – 7.70 (m, 2H), 7.47 – 7.42 (m, 2H), 7.39 – 7.34 (m, 1H), 7.22 (d, J = 3.6 Hz, 1H), 7.17 – 7.14 (m, 1H), 7.14 – 7.12 (m, 1H), 7.12 – 7.09 (m, 2H), 7.10 – 7.07 (m, 1H), 6.77 (d, J = 3.6 Hz, 1H), 6.64 (d, J = 8.6 Hz, 1H), 6.57 (d, J = 8.0 Hz, 1H), 4.89 – 4.82 (m, 1H), 4.69 – 4.61 (m, 1H), 4.22 – 4.15 (m, 2H), 3.17 (dd, J = 13.8, 5.7 Hz, 1H), 3.05 (dd, J = 13.8, 6.7 Hz, 1H), 1.79 – 1.66 (m, 3H), 1.25 (t, J = 7.1 Hz, 3H), 0.97 – 0.95 (m, 3H), 0.95 – 0.93 (m, 3H). ESI-MS [M + Na]$^+$ = 499.3. HPLC t_R = 9.44 min.

Ethyl ((E)-3-(4-chlorophenyl)acryloyl)-L-leucyl-L-phenylalaninate (3i). This product was obtained by reacting 4-chlorocinnamic acid (256 mg, 2 mmol) with **2** (613 mg, 2 mmol) according to procedure A. Flash purification with CH$_2$Cl$_2$/MeOH (0 - 5% MeOH). Yield: 522 mg (79%) of **3i** as a white solid. ^{1}H NMR (400 MHz, CDCl$_3$) δ 7.59 – 7.53 (m, 1H), 7.44 – 7.38 (m, 2H), 7.35 – 7.31 (m, 2H), 7.25 – 7.17 (m, 3H), 7.16 – 7.10 (m, 2H), 6.78 – 6.68 (m, 1H), 6.44 – 6.32 (m, 2H), 4.86 – 4.78 (m, 1H), 4.64 – 4.56 (m, 1H), 4.19 (q, J = 7.1 Hz, 2H), 3.13 (dd, J = 11.8, 5.8 Hz, 1H), 3.06 (dd, J = 14.2, 6.8 Hz, 1H), 1.70 – 1.62 (m, 1H), 1.59 – 1.46 (m, 2H), 1.25 (t, J =

13

7.0 Hz, 3H), 0.94 (d, J = 6.5, 3H), 0.90 (d, J = 6.4 Hz, 3H). ESI-MS [M + Na]$^+$ = 493.4. HPLC t$_R$ = 12.63 min.

Cinnamoyl-L-leucyl-L-phenylalanine (4a). This product was obtained from **3a** (437 mg, 1 mmol) according to procedure B. Yield: 296 mg (73%) of **4a** as a white solid. ^{1}H NMR (400 MHz, CDCl$_3$) δ 7.63 – 7.56 (m, 1H), 7.48 – 7.42 (m, 2H), 7.37 – 7.31 (m, 3H), 7.29 – 7.26 (m, 1H), 7.26 – 7.22 (m, 2H), 7.20 – 7.16 (m, 2H), 7.07 (d, J = 15.0 Hz, 1H), 6.86 – 6.77 (m, 1H), 6.40 (d, J = 15.6 Hz, 1H), 5.04 – 5.02 (m, 1H), 4.85 – 4.79 (m, 1H), 3.15 – 3.06 (m, 2H), 1.58 – 1.44 (m, 3H), 0.93 (d, J = 7.0 Hz, 3H), 0.91 (d, J = 6.6 Hz, 3H). The carboxy proton was not visible. ESI-MS [M - H]$^-$ = 407.2. HPLC t$_R$ = 8.77 min.

(1H-Indole-2-carbonyl)-L-leucyl-L-phenylalanine (4b). This product was obtained from **3b** (448 mg, 1 mmol) according to procedure B. Yield: 397 mg (94%) of **4b** as a light-yellow solid. ^{1}H NMR (400 MHz, DMSO-d_6) δ 12.68 (s, 1H), 11.63 – 11.51 (m, 1H), 8.41 (d, J = 8.5 Hz, 1H), 8.15 (d, J = 7.8 Hz, 1H), 7.62 (d, J = 8.0 Hz, 1H), 7.44 (d, J = 8.2 Hz, 1H), 7.26 – 7.18 (m, 5H), 7.18 – 7.11 (m, 2H), 7.08 – 7.00 (m, 1H), 4.64 – 4.53 (m, 1H), 4.51 – 4.42 (m, 1H), 3.07 (dd, J = 13.9, 5.1 Hz, 1H), 2.95 (dd, J = 13.9, 8.6 Hz, 1H), 1.70 – 1.59 (m, 2H), 1.55 – 1.47 (m, 1H), 0.91 (d, J = 6.3 Hz, 3H), 0.87 (d, J = 6.3 Hz, 3H). ESI-MS [M - H]$^-$ = 420.2. HPLC t$_R$ = 8.64 min.

((E)-3-(4-Chlorophenyl)acryloyl)-L-leucyl-L-phenylalanine (4i). This product was obtained from **3i** (471 mg, 1 mmol) according to procedure B. Yield: 458 mg (97%) of **4i** as a white solid. ^{1}H NMR (400 MHz, CDCl$_3$) δ 7.52 – 7.43 (m, 1H), 7.40 – 7.32 (m, 2H), 7.32 – 7.27 (m, 2H), 7.25 – 7.08 (m, 5H), 6.93 – 6.73 (m, 1H), 6.54 – 6.38 (m, 1H), 4.86 – 4.76 (m, 1H), 3.53 – 3.46 (m, 1H), 3.30 – 3.16 (m, 1H), 2.87 – 2.76 (m, 1H), 2.74 – 2.62 (m, 1H), 1.64 – 1.31 (m, 3H), 0.88 (d, J = 6.1 Hz, 3H), 0.86 (d, J = 6.3 Hz, 3H). The carboxy proton was not visible. ESI-MS [M - H]$^-$ = 441.3. HPLC t$_R$ = 12.56 min.

5-Chloropyridin-3-yl (1H-indole-2-carbonyl)-L-leucyl-L-phenylalaninate (5b). This product was obtained by reacting 3-chloro-5-hydroxypyridine (261 mg, 2 mmol) with **4b** (847 mg, 2 mmol) according to procedure A. Flash purification with CH$_2$Cl$_2$/MeOH (0 - 2% MeOH). Yield: 627 mg (59%) of **5b** as a white solid. Mp: 152–153 °C. ^{1}H NMR (400 MHz, CDCl$_3$) δ 9.77 – 9.51 (m, 1H), 8.50 – 8.32 (m, 1H), 8.15 (d, J = 8.2 Hz, 1H), 7.77 – 7.55 (m, 2H), 7.41 – 7.35 (m, 1H), 7.33 – 7.27 (m, 2H), 7.25 – 7.18 (m, 3H), 7.16 – 7.11 (m, 3H), 6.97 – 6.90 (m, 1H), 6.89 – 6.79 (m, 1H), 5.16 – 5.01 (m, 1H), 4.97 – 4.74 (m, 1H), 3.30 – 3.13 (m, 2H), 1.79 – 1.61 (m, 3H), 1.79 – 1.61 (m, 3H), 0.94 – 0.91 (m, 3H), 0.90 (d, J = 3.9 Hz, 3H). ^{13}C NMR (101 MHz, CDCl$_3$) δ 172.31, 170.11, 161.95, 146.46, 136.74, 136.69, 135.30, 135.12, 129.68, 129.36, 129.03, 128.88, 127.72, 127.63, 125.06, 125.02, 122.26, 120.97, 112.15, 103.55, 53.76, 51.81, 40.94, 37.87, 25.01, 22.93, 22.33. ESI-MS [M + Na]$^+$ = 555.5. HPLC t$_R$ = 9.76 min.

5-Chloropyridin-3-yl (3-(4-chlorophenyl)acryloyl)-L-leucyl-L-phenylalaninate (5i). This product was obtained by reacting 3-chloro-5-hydroxypyridine (258 mg, 2 mmol) with **4i** (883 mg, 2 mmol) according to procedure A. Flash purification with CH$_2$Cl$_2$/MeOH (0 - 2% MeOH). Yield: 121 mg (11%) of **5i** as a white solid. Mp: 64–65 °C. ^{1}H NMR (400 MHz, CDCl$_3$) δ 8.41 – 8.25 (m, 1H), 8.12 – 8.00 (m, 1H), 7.52 – 7.44 (m, 1H), 7.33 – 7.27 (m, 2H), 7.26 – 7.20 (m, 5H), 7.19 – 7.17 (m, 2H), 7.16 – 7.11 (m, 2H), 6.79 – 6.64 (m, 1H), 6.42 – 6.28 (m, 1H), 4.97 – 4.84 (m, 1H), 4.74 – 4.56 (m, 1H), 3.25 – 3.07 (m, 2H), 1.64 – 1.45 (m, 3H), 0.83 (d, J = 5.8 Hz, 3H), 0.81 – 0.77 (m,

3H). ^{13}C NMR (101 MHz, CDCl$_3$) δ 172.69, 169.44, 166.04, 146.89, 146.32, 141.06, 140.70, 135.92, 135.33, 133.14, 131.86, 129.41, 129.33, 129.26, 129.15, 129.01, 127.67, 120.57, 54.05, 51.77, 40.88, 37.88, 24.89, 22.87, 22.32. ESI-MS [M + Na]$^+$ = 576.5. HPLC t$_R$ = 10.34 min.

(S)-2-Cinnamamido-N-((S)-1-((1-cyanocyclopropyl)amino)-1-oxo-3-phenylpropan-2-yl)-4-methylpentanamide (6). This product was obtained by reacting 1-aminocyclopropane-1-carbonitrile × HCl (286 mg, 2 mmol) with **4a** (816 mg, 2 mmol) according to procedure A. Flash purification with CH$_2$Cl$_2$/MeOH (0 - 2% MeOH). Yield: 600 mg (64%) of **6** as a white solid. Mp: 83–84 °C. ^{1}H NMR (400 MHz, DMSO-d_6) δ 8.77 – 8.75 (m, 1H), 8.44 – 8.41 (m, 1H), 8.21 – 8.19 (m, 1H), 7.59 – 7.54 (m, 2H), 7.47 – 7.37 (m, 4H), 7.25 – 7.21 (m, 3H), 7.20 – 7.15 (m, 2H), 6.74 (d, J = 15.8 Hz, 1H), 4.47 – 4.23 (m, 2H), 3.04-3.02 (m, 1H), 2.90 – 2.71 (m, 1H), 1.58 – 1.38 (m, 3H), 1.26 – 1.06 (m, 4H), 0.88 – 0.82 (m, 3H), 0.79 – 0.71 (m, 3H). ^{13}C NMR (101 MHz, DMSO-d_6) δ 172.33, 171.97, 165.13, 139.11, 137.38, 134.82, 129.57, 129.16, 128.95, 127.99, 127.56, 126.29, 121.77, 120.53, 53.69, 51.57, 40.60, 38.22, 24.01, 22.72, 21.91, 19.68, 15.60. ESI-MS [M - H]$^-$ = 471.4. HPLC t$_R$ = 8.51 min.

(S)-2-Cinnamamido-N-((S)-1-((cyanomethyl)amino)-1-oxo-3-phenylpropan-2-yl)-4-methylpentanamide (7). This product was obtained by reacting with 2-aminoacetonitrile hemisulfate (506 mg, 2 mmol) with **4a** (816 mg, 2 mmol) according to procedure A. Flash purification with CH$_2$Cl$_2$/MeOH (0 - 3% MeOH). Yield: 237 mg (22%) of **7** as a white solid. Mp: 221–222 °C. ^{1}H NMR (400 MHz, DMSO-d_6) δ 8.66 – 8.60 (m, 1H), 8.23 – 8.15 (m, 2H), 7.60 – 7.54 (m, 2H), 7.48 – 7.42 (m, 2H), 7.42 – 7.35 (m, 2H), 7.25 – 7.19 (m, 4H), 7.19 – 7.13 (m, 1H), 6.73 (d, J = 15.8 Hz, 1H), 4.52 – 4.44 (m, 1H), 4.44 – 4.36 (m, 1H), 4.14 (d, J = 5.6 Hz, 2H), 3.01 (dd, J = 13.8, 5.3 Hz, 1H), 2.86 (dd, J = 13.7, 9.0 Hz, 1H), 1.59 – 1.51 (m, 1H), 1.45 – 1.38 (m, 2H), 0.87 (d, J = 6.6 Hz, 3H), 0.83 (d, J = 6.5 Hz, 3H). ^{13}C NMR (101 MHz, DMSO-d_6) δ 171.93, 171.49, 165.02, 139.06, 137.37, 134.89, 129.47, 129.11, 128.94, 128.06, 127.50, 126.29, 121.92, 117.29, 53.67, 51.26, 40.63, 37.02, 27.04, 24.12, 22.96, 21.59. ESI-MS [M + Na]$^+$ = 469.4. HPLC t$_R$ = 8.17 min.

(S)-2-Cinnamamido-N-((S)-1-hydroxy-3-phenylpropan-2-yl)-4-methylpentanamide (8a). This product was obtained from **3a** (218 mg, 0.5 mmol) according to procedure F. Yield: 175 mg (89%) of **8a** as a white solid. ^{1}H NMR (400 MHz, CDCl$_3$) δ 7.62 (d, J = 15.6 Hz, 1H), 7.50 – 7.45 (m, 2H), 7.36 – 7.33 (m, 3H), 7.22 – 7.17 (m, 4H), 7.16 – 7.11 (m, 1H), 7.03 – 6.98 (m, 1H), 6.46 (d, J = 8.3 Hz, 1H), 6.42 (d, J = 15.6 Hz, 1H), 4.63 – 4.55 (m, 1H), 4.21 – 4.12 (m, 1H), 3.70 (dd, J = 11.2, 3.7 Hz, 1H), 3.64 (dd, J = 11.1, 5.0 Hz, 1H), 2.92 – 2.85 (m, 2H), 1.73 – 1.56 (m, 3H), 0.94 (d, J = 6.2 Hz, 3H), 0.92 (d, J = 6.1 Hz, 3H), 0.87 – 0.80 (m, 1H). ESI-MS [M + Na]$^+$ = 417.4. HPLC t$_R$ = 8.51 min.

N-((S)-1-(((S)-1-Hydroxy-3-phenylpropan-2-yl)amino)-4-methyl-1-oxopentan-2-yl)-1H-indole-2-carboxamide (8b). This product was obtained from **3b** (226 mg, 0.5 mmol) according to procedure F. Flash purification with petroleum ether/EtOAc (0 - 70% EtOAc). Yield: 207 mg (100%) of **8b** as a white solid. ^{1}H NMR (400 MHz, CDCl$_3$) δ 9.88 (s, 1H), 7.61 – 7.59 (m, 1H), 7.41 – 7.33 (m, 1H), 7.29 – 7.23 (m, 2H), 7.21 – 7.19 (m, 1H), 7.16 – 7.09 (m, 3H), 7.03 – 6.97 (m, 2H), 4.86 – 4.62 (m, 1H), 4.37 – 4.17 (m, 1H), 3.84 – 3.54 (m, 1H), 3.52 – 3.43 (m, 1H),

2.94 – 2.81 (m, 2H), 1.72 – 1.69 (m, 1H), 1.31 – 1.19 (m, 2H), 0.89 (d, *J* = 6.2 Hz, 3H), 0.86 (d, *J* = 5.8 Hz, 3H), 0.81 (t, *J* = 6.0 Hz, 1H). ESI-MS [M - H]$^-$ = 406.2. HPLC t$_R$ = 12.17 min.

(S)-2-((E)-3-(3,5-Dimethoxyphenyl)acrylamido)-N-((S)-1-hydroxy-3-phenylpropan-2-yl)-4-methylpentanamide (8c). This product was obtained from **3c** (248 mg, 0.5 mmol) according to the procedure F. Yield: 179 mg (79%) of **8c** as a white solid. ^{1}H NMR (400 MHz, CDCl$_3$) δ 7.56 – 7.51 (m, 1H), 7.27 – 7.23 (m, 2H), 7.22 – 7.18 (m, 3H), 7.11 – 7.07 (m, 1H), 6.64 – 6.59 (m, 2H), 6.53 (d, *J* = 8.0 Hz, 1H), 6.47 – 6.43 (m, 1H), 6.40 (d, *J* = 15.6 Hz, 1H), 4.61 – 4.50 (m, 1H), 4.28 – 4.12 (m, 1H), 3.78 – 3.74 (m, 6H), 3.72 – 3.67 (m, 1H), 3.63 (dd, *J* = 11.2, 5.0 Hz, 1H), 2.91 – 2.85 (m, 2H), 1.68 – 1.57 (m, 2H), 1.49 – 1.44 (m, 1H), 0.91 (d, *J* = 5.9 Hz, 3H), 0.90 (d, *J* = 5.8 Hz, 3H), 0.84 – 0.82 (m, 1H). ESI-MS [M + Na]$^+$ = 477.4. HPLC t$_R$ = 8.77 min.

(S)-2-Cinnamamido-4-methyl-N-((S)-1-oxo-3-phenylpropan-2-yl)pentanamide (9a). This product was obtained from **8a** (197 mg, 0.5 mmol) according to procedure G. Flash purification with PE/EA (0 – 50% EA). Yield: 187 mg (95%) of **9a** as a white solid. Mp: 75–76 °C. ^{1}H NMR (400 MHz, CDCl$_3$) δ 9.60 (s, 1H), 7.62 (d, *J* = 15.6 Hz, 1H), 7.52 – 7.47 (m, 2H), 7.39 – 7.35 (m, 3H), 7.26 – 7.21 (m, 2H), 7.20 – 7.13 (m, 3H), 7.00 (d, *J* = 7.1 Hz, 1H), 6.40 (d, *J* = 15.6 Hz, 1H), 6.26 (d, *J* = 14.4 Hz, 1H), 4.76 – 4.57 (m, 2H), 3.16 (dd, *J* = 14.1, 6.4 Hz, 1H), 3.06 (dd, *J* = 14.2, 7.3 Hz, 1H), 1.74 – 1.63 (m, 2H), 1.61 – 1.55 (m, 1H), 0.94 (d, *J* = 6.3 Hz, 3H), 0.93 (d, *J* = 6.1 Hz, 3H). ^{13}C NMR (101 MHz, CDCl$_3$) δ 198.74, 172.59, 166.13, 142.19, 135.74, 134.72, 130.11, 129.42, 129.04, 128.90, 128.04, 127.21, 120.00, 59.95, 51.73, 41.03, 35.17, 24.97, 22.98, 22.32. ESI-MS [M + Na]$^+$ = 415.3. HPLC t$_R$ = 8.64 min.

N-((S)-4-Methyl-1-oxo-1-(((S)-1-oxo-3-phenylpropan-2-yl)amino)pentan-2-yl)-1H-indole-2-carboxamide (9b). This product was obtained from **8b** (207 mg, 0.5 mmol) according to procedure G. Flash purification with CH$_2$Cl$_2$/MeOH (0 - 3% MeOH). Yield: 41 mg (20%) of **9b** as a white solid. Mp: 81–82 °C. ^{1}H NMR (400 MHz, CDCl$_3$) δ 9.66 – 9.56 (m, 1H), 9.51 – 9.37 (m, 1H), 7.68 – 7.62 (m, 1H), 7.45 – 7.38 (m, 1H), 7.34 – 7.28 (m, 1H), 7.23 – 7.17 (m, 2H), 7.16 – 7.11 (m, 2H), 7.11 – 7.06 (m, 2H), 6.96 – 6.92 (m, 1H), 6.91 – 6.84 (m, 1H), 4.87 – 4.67 (m, 2H), 3.50 – 3.47 (m, 1H), 3.20 – 3.03 (m, 2H), 1.74 – 1.61 (m, 3H), 0.93 (d, *J* = 7.0 Hz, 3H), 0.90 (d, *J* = 7.8 Hz, 3H). ^{13}C NMR (101 MHz, CDCl$_3$) δ 198.55, 172.19, 161.61, 136.50, 135.39, 129.17, 128.71, 127.61, 127.16, 127.06, 124.88, 122.12, 120.84, 111.94, 103.27, 59.76, 51.63, 41.17, 35.00, 24.90, 22.80, 22.18. ESI-MS [M - H]$^-$ = 404.2. HPLC t$_R$ = 8.61 min.

(S)-2-((E)-3-(3,5-Dimethoxyphenyl)acrylamido)-4-methyl-N-((S)-1-oxo-3-phenylpropan-2-yl)pentanamide (9c). This product was obtained from **8c** (225 mg, 0.5 mmol) according to procedure G. Flash purification with CH$_2$Cl$_2$/MeOH (0 - 5% MeOH). Yield: 129 mg (57%) of **9c** as a white solid. Mp: 70–71 °C. ^{1}H NMR (400 MHz, CDCl$_3$) δ 9.62 – 9.59 (m, 1H), 7.45 (d, *J* = 15.6 Hz, 1H), 7.21 – 7.13 (m, 3H), 7.12 – 7.05 (m, 2H), 6.94 – 6.83 (m, 1H), 6.60 – 6.53 (m, 2H), 6.44 – 6.36 (m, 1H), 6.37 (d, *J* = 15.5 Hz, 1H), 6.24 (d, *J* = 8.3 Hz, 1H), 4.69 – 4.59 (m, 2H), 3.82 – 3.77 (m, 6H), 3.16 (dd, *J* = 14.0, 6.6 Hz, 1H), 3.06 (dd, *J* = 14.1, 7.3 Hz, 1H), 1.69 – 1.52 (m, 3H), 0.95 – 0.91 (m, 3H), 0.91 – 0.86 (m, 3H). ^{13}C NMR (101 MHz, CDCl$_3$) δ 198.79, 172.50, 165.99, 161.17, 161.14, 142.10, 136.63, 135.75, 129.42, 128.90, 127.21, 120.59, 106.01, 59.95, 55.54,

51.71, 41.01, 35.15, 24.94, 22.99, 22.28. ESI-MS [M + Na]$^+$ = 475.3. HPLC t$_R$ = 11.16 min.

N-((S)-1-(((S)-1-Amino-1-oxo-3-phenylpropan-2-yl)amino)-4-methyl-1-oxopentan-2-yl)-1H-indole-2-carboxamide (10b). This product was obtained from **3b** (449 mg, 1 mmol) according to procedure D. Yield: 400 mg (95%) of **10b** as a white solid. Flash purification with CH$_2$Cl$_2$/MeOH (0 - 7% MeOH). ^{1}H NMR (400 MHz, CDCl$_3$) δ 8.42 (d, *J* = 8.0 Hz, 1H), 7.90 (d, J = 8.3 Hz, 1H), 7.63 (d, J = 7.9 Hz, 1H), 7.47 – 7.42 (m, 1H), 7.36 (s, 1H), 7.26 – 7.23 (m, 1H), 7.22 – 7.18 (m, 3H), 7.18 – 7.15 (m, 2H), 7.15 – 7.08 (m, 2H), 7.08 – 7.00 (m, 2H), 4.55 – 4.41 (m, 2H), 3.03 (dd, *J* = 13.8, 5.0 Hz, 1H), 2.84 (dd, *J* = 13.8, 8.8 Hz, 1H), 1.68 – 1.55 (m, 2H), 1.53 – 1.41 (m, 1H), 0.90 (d, *J* = 6.3 Hz, 3H), 0.85 (d, *J* = 6.3 Hz, 3H). ESI-MS [M - H]$^-$ = 419.2. HPLC t$_R$ = 7.65 min.

(S)-N-((S)-1-Amino-1-oxo-3-phenylpropan-2-yl)-2-((E)-3-(3,5-dimethoxyphenyl)acrylamido)-4-methylpentanamide (10c). This product was obtained from **3c** (500 mg, 1 mmol) according to procedure D. Flash purification with CH$_2$Cl$_2$/MeOH (0 - 7% MeOH). Yield: 376 mg (81%) of **10c** as a white solid. ^{1}H NMR (400 MHz, DMSO-d$_6$) δ 8.19 – 8.12 (m, 1H), 7.95 (d, *J* = 8.3 Hz, 1H), 7.41 – 7.30 (m, 2H), 7.24 – 7.19 (m, 4H), 7.17 – 7.13 (m, 1H), 7.11 – 7.06 (m, 1H), 6.76 – 6.70 (m, 3H), 6.55 – 6.49 (m, 1H), 4.46 – 4.38 (m, 1H), 4.38 – 4.29 (m, 1H), 3.78 – 3.76 (m, 6H), 3.02 (dd, *J* = 13.8, 4.8 Hz, 1H), 2.83 (dd, *J* = 13.8, 9.2 Hz, 1H), 1.58 – 1.51 (m, 1H), 1.45 – 1.35 (m, 2H), 0.86 (d, *J* = 6.6 Hz, 3H), 0.82 (d, *J* = 6.5 Hz, 3H). ESI-MS [M + Na]$^+$ = 490.3. HPLC t$_R$ = 8.41 min.

(S)-N-((S)-1-amino-1-oxo-3-phenylpropan-2-yl)-2-(2-(4-chlorophenoxy)acetamido)-4-methylpentanamide (10d). This product was obtained from **3d** (474 mg, 1 mmol) according to procedure D. Yield: 407 mg (91%) of **10d** as a white solid. ^{1}H NMR (400 MHz, CDCl$_3$) δ 8.05 (d, *J* = 8.2 Hz, 1H), 7.94 (d, *J* = 8.3 Hz, 1H), 7.37 – 7.29 (m, 3H), 7.25 – 7.15 (m, 5H), 7.07 (s, 1H), 6.99 – 6.92 (m, 2H), 4.52 – 4.50 (m, 2H), 4.46 – 4.41 (m, 1H), 4.33 – 4.26 (m, 1H), 3.01 (dd, *J* = 13.8, 5.0 Hz, 1H), 2.81 (dd, *J* = 13.8, 9.0 Hz, 1H), 1.47 – 1.34 (m, 3H), 0.82 (d, *J* = 6.2 Hz, 3H), 0.78 (d, *J* = 6.2 Hz, 3H). ESI-MS [M + Na]$^+$ = 468.2. HPLC t$_R$ = 8.22 min.

(S)-N-((S)-1-Amino-1-oxo-3-phenylpropan-2-yl)-2-(2-(2,4-dichlorophenoxy)acetamido)-4-methylpentanamide (10e). This product was obtained from **3e** (475 mg, 1 mmol) according to procedure G. Yield: 552 mg (78%) of **10e** as a light brown solid. ^{1}H NMR (400 MHz, CDCl$_3$) δ 7.46 – 7.43 (m, 1H), 7.26 – 7.19 (m, 5H), 7.17 – 7.12 (m, 1H), 7.01 (d, *J* = 7.1 Hz, 1H), 6.81 (d, *J* = 8.8 Hz, 1H), 6.62 (d, *J* = 7.7 Hz, 1H), 6.00 – 5.93 (m, 1H), 5.40 – 5.34 (m, 1H), 4.71 – 4.64 (m, 1H), 4.46 – 4.29 (m, 3H), 3.15 – 3.07 (m, 2H), 1.75 – 1.67 (m, 1H), 1.58 – 1.53 (m, 2H), 0.93 (d, *J* = 6.3 Hz, 3H), 0.90 (d, *J* = 6.3 Hz, 3H). ESI-MS [M + Na]$^+$ = 502.2. HPLC t$_R$ = 9.14 min.

(S)-N-((S)-1-Amino-1-oxo-3-phenylpropan-2-yl)-2-(2-(3-(dimethylamino)phenoxy)acetamido)-4-methylpentanamide (10f). This product was obtained from **3f** (483 mg, 1 mmol) according to procedure D. Yield: 454 mg (100%) of **10f** as a white solid. ^{1}H NMR (400 MHz, DMSO-d_6) δ 8.01 (d, *J* = 8.4 Hz, 1H), 7.94 (d, *J* = 8.3 Hz, 1H), 7.36 (s, 1H), 7.25 – 7.15 (m, 5H), 7.09 – 7.03 (m, 2H), 6.36 – 6.32 (m, 1H), 6.27 – 6.25 (m, 1H), 6.25 – 6.21 (m, 1H), 4.51 – 4.40 (m, 3H), 4.36 – 4.29 (m, 1H), 3.00 (dd, *J* = 13.8, 5.1 Hz, 1H), 2.86 (s, 6H), 2.81 (dd, *J* = 13.8, 9.1 Hz, 1H), 1.46 – 1.34 (m, 3H), 0.81 (d, *J* = 6.2 Hz, 3H),

15

0.78 (d, J = 6.2 Hz, 3H). ESI-MS [M + Na]$^+$ = 477.1. HPLC t$_R$ = 7.14 min.

(R,S)-N-((S)-1-(((S)-1-Amino-1-oxo-3-phenylpropan-2-yl)amino)-4-methyl-1-oxopentan-2-yl)chromane-2-carboxamide (10g). This product was obtained from **3g** (464 mg, 1 mmol) according to procedure D. Yield: 438 mg (100%) of **10g** as a white solid. ^{1}H NMR (400 MHz, DMSO-d_6) δ 8.03 – 7.74 (m, 2H), 7.44 – 7.33 (m, 1H), 7.26 – 7.14 (m, 5H), 7.12 – 7.02 (m, 3H), 6.88 – 6.81 (m, 2H), 4.63 – 4.52 (m, 1H), 4.49 – 4.40 (m, 1H), 4.34 – 4.25 (m, 1H), 3.04 – 2.95 (m, 1H), 2.86 – 2.58 (m, 3H), 2.15 – 2.04 (m, 1H), 2.00 – 1.79 (m, 1H), 1.54 – 1.25 (m, 3H), 0.90 – 0.80 (m, 3H), 0.78 – 0.70 (m, 3H). ESI-MS [M + Na]$^+$ = 460.1. HPLC t$_R$ = 8.30 min.

N-((S)-1-(((S)-1-Amino-1-oxo-3-phenylpropan-2-yl)amino)-4-methyl-1-oxopentan-2-yl)-5-phenylfuran-2-carboxamide (10h). This product was obtained from **3h** (476 mg, 1 mmol) according to the procedure D. Yield: 447 mg (100%) of **10h** as a white solid. Flash purification with CH$_2$Cl$_2$/MeOH (0 - 7% MeOH). ^{1}H NMR (400 MHz, DMSO-d_6) δ 8.44 (d, J = 8.1 Hz, 1H), 7.98 – 7.90 (m, 3H), 7.52 – 7.45 (m, 2H), 7.42 – 7.35 (m, 2H), 7.25 (d, J = 3.6 Hz, 1H), 7.21 – 7.14 (m, 4H), 7.13 – 7.08 (m, 3H), 4.49 – 4.41 (m, 2H), 3.02 (dd, J = 13.8, 4.9 Hz, 1H), 2.84 (dd, J = 13.8, 8.9 Hz, 1H), 1.68 – 1.55 (m, 2H), 1.52 – 1.45 (m, 1H), 0.89 (d, J = 6.3 Hz, 3H), 0.84 (d, J = 6.3 Hz, 3H). ESI-MS [M + Na]$^+$ = 470.1. HPLC t$_R$ = 8.79 min.

(S)-2-Cinnamamido-N-((S)-1-cyano-2-phenylethyl)-4-methylpentanamide (11a). To a solution of **9a** (400 mg, 1 mmol), NH$_2$OH × HCl (140 mg, 1.02 mmol) in pyridine (dry), TiCl$_4$ (484 mg, 0.28 mL, 2.56 mmol) was added. The reaction mixture was stirred at 40 °C for 3 h. After reaction control through TLC, it was cooled to room temperature and treated with a 5% aq. NaHSO$_4$ solution (3 mL). This mixture was extracted with CH$_2$Cl$_2$ (3 × 15 mL). The combined organic phases were washed with brine (15 mL), dried over Na$_2$SO$_4$, filtered, and evaporated to dryness. Flash purification with petroleum ether/EtOAc (0 - 70% EtOAc). Yield: 84 mg (22%) of **11a** as a yellow solid. Mp: 65–66 °C. ^{1}H NMR (400 MHz, CDCl$_3$) δ 8.11 – 8.04 (m, 1H), 7.69 – 7.62 (m, 1H), 7.53 – 7.46 (m, 2H), 7.38 – 7.32 (m, 3H), 7.31 – 7.28 (m, 1H), 7.25 – 7.16 (m, 4H), 6.63 (d, J = 8.4 Hz, 1H), 6.47 (d, J = 15.6 Hz, 1H), 5.13 – 5.01 (m, 1H), 4.78 – 4.65 (m, 1H), 3.18 – 3.01 (m, 2H), 1.74 – 1.61 (m, 2H), 1.57 – 1.47 (m, 1H), 0.95 (d, J = 6.5 Hz, 3H), 0.93 (d, J = 6.4 Hz, 3H). ^{13}C NMR (101 MHz, CDCl$_3$) δ 172.27, 166.45, 142.40, 134.54, 134.20, 130.23, 129.53, 129.06, 128.96, 128.11, 127.83, 119.91, 118.24, 51.79, 42.15, 40.93, 39.00, 24.97, 22.91, 22.39. ESI-MS [M + Na]$^+$ = 412.3. HPLC t$_R$ = 8.64 min.

N-((S)-1-(((S)-1-Cyano-2-phenylethyl)amino)-4-methyl-1-oxopentan-2-yl)-1H-indole-2-carboxamide (11b). This product was obtained from **10b** (423 mg, 1 mmol) according to procedure D. Flash purification with petroleum ether/EtOAc (0 - 50% EtOAc). Yield: 177 mg (44%) of **11b** as a white solid. Mp: 57–58°C. ^{1}H NMR (400 MHz, CDCl$_3$) δ 9.71 – 9.36 (m, 1H), 7.87 (d, J = 8.5 Hz, 1H), 7.66 (d, J = 8.1 Hz, 1H), 7.49 – 7.41 (m, 1H), 7.36 – 7.29 (m, 1H), 7.28 – 7.21 (m, 2H), 7.19 – 7.08 (m, 4H), 7.01 – 6.96 (m, 1H), 6.96 – 6.85 (m, 1H), 5.21 – 5.05 (m, 1H), 4.84 – 4.63 (m, 1H), 3.16 – 2.99 (m, 2H), 1.79 – 1.67 (m, 3H), 0.94 – 0.90 (m, 3H), 0.90 – 0.84 (m, 3H). ^{13}C NMR (101 MHz, CDCl$_3$) δ 171.90, 162.01, 136.75, 133.83, 129.50, 129.07, 128.88, 127.89, 127.65, 125.24, 122.32,

121.12, 118.67, 112.20, 104.06, 60.57, 51.69, 42.06, 40.79, 24.98, 22.90, 22.28. ESI-MS [M + Na]$^+$ = 425.0. HPLC t$_R$ = 8.20 min.

(S)-N-((S)-1-Cyano-2-phenylethyl)-2-((E)-3-(3,5-dimethoxyphenyl)acrylamido)-4-methylpentanamide (11c). This product was obtained from **10c** (463 mg, 1 mmol) according to procedure E. Flash purification with petroleum ether/EtOAc (0 - 70% EtOAc). Yield: 190 mg (42%) of **11c** as a white solid. Mp: 73–74 °C. ^{1}H NMR (400 MHz, CDCl$_3$) δ 8.84 (d, J = 8.3 Hz, 1H), 7.67 (d, J = 15.6 Hz, 1H), 7.38 – 7.29 (m, 2H), 7.28 – 7.21 (m, 4H), 6.78 – 6.72 (m, 2H), 6.61 (d, J = 15.6 Hz, 1H), 6.53 – 6.47 (m, 1H), 5.20 – 5.11 (m, 1H), 5.03 – 4.94 (m, 1H), 3.78 (s, 6H), 3.21 – 3.05 (m, 2H), 1.84 – 1.73 (m, 3H), 1.04 (d, J = 6.4 Hz, 3H), 1.02 (d, J = 6.6 Hz, 3H). ^{13}C NMR (101 MHz, CDCl$_3$) δ 172.84, 166.33, 161.08, 142.14, 136.48, 134.31, 129.47, 128.82, 127.72, 120.58, 118.33, 106.03, 102.32, 55.40, 51.97, 42.37, 41.51, 39.06, 25.01, 22.80, 22.49. ESI-MS [M + Na]$^+$ = 472.2. HPLC t$_R$ = 8.73 min.

(S)-2-(2-(4-Chlorophenoxy)acetamido)-N-((S)-1-cyano-2-phenylethyl)-4-methylpentanamide (11d). This product was obtained from **10d** (447 mg, 1 mmol) according to procedure E. Flash purification with petroleum ether/EtOAc (0 - 70% EtOAc). Yield: 225 mg (53%) of **11d** as a white solid. Mp: 145–146 °C. ^{1}H NMR (400 MHz, CDCl$_3$) δ 7.25 – 7.19 (m, 5H), 7.19 – 7.14 (m, 3H), 6.80 – 6.75 (m, 2H), 6.75 – 6.72 (m, 1H), 5.08 – 5.00 (m, 1H), 4.53 – 4.44 (m, 1H), 4.38 – 4.32 (m, 1H), 4.25 – 4.19 (m, 1H), 3.07 – 2.99 (m, 2H), 1.64 – 1.59 (m, 1H), 1.54 – 1.44 (m, 2H), 0.84 (d, J = 6.7 Hz, 3H), 0.82 (d, J = 6.6 Hz, 3H). ^{13}C NMR (101 MHz, CDCl$_3$) δ 171.01, 168.53, 155.54, 133.97, 129.92, 129.58, 129.01, 128.05, 127.61, 118.03, 116.12, 67.29, 51.09, 41.81, 40.27, 38.89, 24.81, 22.86, 22.20. ESI-MS [M + Na]$^+$ = 450.2. HPLC t$_R$ = 9.11 min.

(S)-N-((S)-1-Cyano-2-phenylethyl)-2-(2-(2,4-dichlorophenoxy)acetamido)-4-methylpentanamide (11e). This product was obtained from **10e** (484 mg, 1 mmol) according to procedure E. Flash purification with petroleum ether/EtOAc (0 - 70% EtOAc). Yield: 362 mg (78%) of **11e** as a white solid. Mp: 146–147°C. ^{1}H NMR (400 MHz, CDCl$_3$) δ 7.39 (d, J = 3.8 Hz, 1H), 7.28 – 7.23 (m, 2H), 7.23 – 7.20 (m, 3H), 7.20 – 7.18 (m, 1H), 7.15 (d, J = 8.6 Hz, 1H), 6.99 (d, J = 8.0 Hz, 1H), 6.77 (d, J = 8.8 Hz, 1H), 5.12 – 5.06 (m, 1H), 4.51 – 4.40 (m, 2H), 4.33 – 4.25 (m, 1H), 3.06 (d, J = 6.8 Hz, 2H), 1.74 – 1.68 (m, 1H), 1.61 – 1.53 (m, 2H), 0.90 (d, J = 6.3 Hz, 3H), 0.87 (d, J = 6.3 Hz, 3H). ^{13}C NMR (101 MHz, CDCl$_3$) δ 170.87, 168.06, 151.43, 133.98, 130.47, 129.56, 129.01, 128.22, 128.02, 127.95, 124.03, 118.07, 114.86, 68.06, 51.29, 41.73, 40.12, 38.88, 24.85, 22.94, 22.17. ESI-MS [M + Na]$^+$ = 484.2. HPLC t$_R$ = 9.84 min.

(S)-N-((S)-1-Cyano-2-phenylethyl)-2-(2-(3-(dimethylamino)phenoxy)acetamido)-4-methylpentanamide (11f). This product was obtained from **10f** (454 mg, 1 mmol) according to procedure E. Flash purification with petroleum ether/EtOAc (0 - 70% EtOAc). Yield: 305 mg (70%) of **11f** as a yellow solid. Mp: 68–69 °C. ^{1}H NMR (400 MHz, CDCl$_3$) δ 7.33 – 7.28 (m, 2H), 7.26 – 7.24 (m, 1H), 7.24 – 7.20 (m, 2H), 7.19 – 7.14 (m, 1H), 7.09 (d, J = 8.4 Hz, 1H), 6.76 (d, J = 8.3 Hz, 1H), 6.45 – 6.40 (m, 1H), 6.27 – 6.25 (m, 1H), 6.24 – 6.20 (m, 1H), 5.12 – 5.04 (m, 1H), 4.56 – 4.46 (m, 2H), 4.40 – 4.32 (m, 1H), 3.11 – 3.00 (m, 2H), 2.96 (s, 6H), 1.75 – 1.67 (m, 1H), 1.58 – 1.48 (m, 2H), 0.89 (d, J = 6.7 Hz, 3H), 0.88 (d, J = 6.8 Hz, 3H). ^{13}C NMR (101 MHz, CDCl$_3$) δ 171.03, 169.47,

158.20, 152.23, 134.00, 130.33, 129.51, 129.02, 128.04, 118.04, 107.11, 101.64, 99.44, 67.00, 51.01, 41.68, 40.61, 39.89, 38.91, 24.72, 22.93, 22.09. ESI-MS [M + Na]$^+$ = 459.2. HPLC t$_R$ = 7.82 min.

(R,S)-N-((S)-1-(((S)-1-Cyano-2-phenylethyl)amino)-4-methyl-1-oxopentan-2-yl)chromane-2-carboxamide (11g). This product was obtained from **10g** (438 mg, 1 mmol) according to procedure E. Flash purification with petroleum ether/EtOAc (0 - 50% EtOAc). Yield: 323 mg (77%) of **11g** as a white solid. Mp: 149–150°C. ^{1}H NMR (400 MHz, CDCl$_3$) δ 7.36 – 7.27 (m, 3H), 7.27 – 7.21 (m, 3H), 7.19 – 7.12 (m, 1H), 7.08 – 7.06 (m, 1H), 6.96 – 6.88 (m, 2H), 6.87 – 6.79 (m, 1H), 5.16 – 5.01 (m, 1H), 4.58 – 4.37 (m, 2H), 3.10-3.06 (m, 2H), 2.93 – 2.84 (m, 1H), 2.75 – 2.73 (m, 1H), 2.41 – 2.31 (m, 1H), 2.05 – 1.85 (m, 1H), 1.77 – 1.49 (m, 3H), 0.94 (d, *J* = 6.4 Hz, 3H), 0.83 (d, *J* = 6.4 Hz, 3H). ^{13}C NMR (101 MHz, CDCl$_3$) δ 171.68, 171.07, 152.76, 133.93, 130.00, 129.54, 129.10, 128.08, 127.88, 122.01, 121.76, 117.98, 116.87, 75.22, 51.49, 51.05, 41.78, 41.76, 40.01, 39.73, 39.00, 38.95, 25.02, 24.82, 24.00, 22.94, 22.09. ESI-MS [M + Na]$^+$ = 442.2. HPLC t$_R$ = 9.15 min.

N-((S)-1-(((S)-1-Cyano-2-phenylethyl)amino)-4-methyl-1-oxopentan-2-yl)-5-phenylfuran-2-carboxamide (11h). This product was obtained from **10h** (426 mg, 1 mmol) according to procedure E. Flash purification with petroleum ether/EtOAc (0 - 50% EtOAc). Yield: 356 mg (87%) of **11h** as a white solid. Mp: 77–78 °C. ^{1}H NMR (400 MHz, CDCl$_3$) δ 7.75 – 7.70 (m, 2H), 7.56 (d, *J* = 8.5 Hz, 1H), 7.49 – 7.43 (m, 2H), 7.41 – 7.37 (m, 1H), 7.27 (d, *J* = 3.6 Hz, 1H), 7.22 – 7.15 (m, 5H), 6.79 (d, *J* = 3.6 Hz, 1H), 6.65 (d, *J* = 8.5 Hz, 1H), 5.18 – 5.11 (m, 1H), 4.76 – 4.69 (m, 1H), 3.11 – 3.05 (m, 2H), 1.84 – 1.79 (m, 1H), 1.75 – 1.69 (m, 2H), 0.98 (d, *J* = 6.4 Hz, 3H), 0.96 (d, *J* = 6.4 Hz, 3H). ^{13}C NMR (101 MHz, CDCl$_3$) δ 171.49, 158.70, 156.41, 145.95, 133.96, 129.49, 129.45, 129.20, 129.11, 128.90, 127.85, 124.79, 118.21, 117.85, 107.66, 51.12, 41.78, 40.41, 39.11, 24.93, 22.97, 22.35. ESI-MS [M + Na]$^+$ = 452.1. HPLC t$_R$ = 9.24 min.

(S)-2-Cinnamamido-4-methyl-N-((S)-1-phenyl-4-(phenylsulfonyl)but-3-en-2-yl)pentanamide (12a). This product was obtained by reacting **9a** (197 mg, 0.5 mmol) with diethyl ((phenylsulfonyl)methyl)phosphonate (154 mg, 0.5 mmol) according to procedure H. Flash purification with petroleum ether/EtOAc (0 - 70% EtOAc). Yield: 103 mg (39%) of **12a** as a white solid. Mp: 90–91 °C. ^{1}H NMR (400 MHz, DMSO-*d$_6$*) δ 8.29 – 8.11 (m, 2H), 7.89 – 7.82 (m, 1H), 7.79 – 7.76 (m, 1H), 7.74 – 7.67 (m, 1H), 7.64 – 7.60 (m, 1H), 7.60 – 7.54 (m, 3H), 7.46 – 7.37 (m, 4H), 7.25 – 7.11 (m, 5H), 6.97 – 6.87 (m, 1H), 6.73 (d, *J* = 15.9 Hz, 1H), 6.65 (d, *J* = 15.1, Hz, 1H), 4.80 – 4.69 (m, 1H), 4.33 – 4.18 (m, 1H), 3.07 – 2.90 (m, 1H), 2.89 – 2.65 (m, 1H), 1.54 – 1.42 (m, 1H), 1.36 – 1.31 (m, 1H), 1.25 – 1.15 (m, 1H), 0.84 (d, *J* = 6.6 Hz, 3H), 0.78 (d, *J* = 6.5 Hz, 3H). ^{13}C NMR (101 MHz, DMSO-*d$_6$*) δ 171.52, 164.85, 146.15, 140.19, 138.80, 138.75, 137.31, 134.89, 133.54, 130.11, 129.50, 129.20, 128.92, 128.05, 127.44, 126.99, 126.23, 122.05, 51.55, 50.40, 40.72, 38.51, 24.14, 22.65, 21.65. ESI-MS [M + Na]$^+$ = 553.4. HPLC t$_R$ = 8.96 min and 9.23 min (*E/Z* mixture).

N-((S)-4-Methyl-1-oxo-1-(((S)-1-phenyl-4-(phenylsulfonyl)but-3-en-2-yl)amino)pentan-2-yl)-1H-indole-2-carboxamide (12b). This product was obtained by reacting **9b** (204 mg, 0.5 mmol) with diethyl ((phenylsulfonyl)methyl)phosphonate (154 mg, 0.5 mmol)

according to procedure H. Flash purification with petroleum ether/EtOAc (0 - 70% EtOAc). Yield: 194 mg (71%) of **12b** as a white solid. Mp: 115–116 °C. ^{1}H NMR (400 MHz, DMSO-*d$_6$*) δ 11.60 – 11.47 (m, 1H), 8.44 – 8.19 (m, 2H), 7.99 – 7.91 (m, 1H), 7.87 – 7.81 (m, 1H), 7.79 – 7.73 (m, 1H), 7.73 – 7.65 (m, 1H), 7.65 – 7.55 (m, 3H), 7.50 – 7.45 (m, 1H), 7.29 – 7.24 (m, 1H), 7.24 – 7.21 (m, 2H), 7.21 – 7.19 (m, 1H), 7.18 – 7.14 (m, 2H), 7.08 – 7.02 (m, 1H), 7.01 – 6.89 (m, 1H), 6.88 – 6.60 (m, 1H), 4.83 – 4.69 (m, 1H), 4.47 – 4.41 (m, 1H), 3.07 – 2.90 (m, 1H), 2.88 – 2.66 (m, 1H), 1.61 – 1.50 (m, 1H), 1.43 – 1.22 (m, 2H), 0.88 – 0.81 (m, 3H), 0.81 – 0.73 (m, 3H). ^{13}C NMR (101 MHz, DMSO-*d$_6$*) δ 171.76, 161.03, 146.44, 140.49, 140.19, 137.60, 136.47, 133.77, 129.48, 129.24, 129.01, 128.06, 127.80, 127.04, 126.28, 123.44, 121.52, 119.71, 112.26, 103.63, 51.87, 50.66, 40.05, 38.62, 24.12, 22.68, 21.67. ESI-MS [M + Na]$^+$ = 566.3. HPLC t$_R$ = 8.93 min and 9.19 min (*E/Z* mixture).

(S)-4-((S)-2-Cinnamamido-4-methylpentanamido)-5-phenylpent-2-enamide (13a). This product was obtained by reacting **9a** (296 mg, 0.5 mmol) with diethyl (2-amino-2-oxoethyl)phosphonate (146 mg, 0.75 mmol) according to procedure I. Flash purification with CH$_2$Cl$_2$/MeOH (0 - 7% MeOH). Yield: 103 mg (48%) of **13a** as a white solid. Mp: 186-187 °C. ^{1}H NMR (400 MHz, DMSO-*d$_6$*) δ 8.28 – 8.24 (m, 1H), 8.16 – 8.09 (m, 1H), 7.59 – 7.53 (m, 2H), 7.47 – 7.37 (m, 5H), 7.28 – 7.21 (m, 4H), 7.19 – 7.12 (m, 1H), 7.00 – 6.94 (m, 1H), 6.78 – 6.72 (m, 1H), 6.65 – 6.52 (m, 1H), 5.98 – 5.81 (m, 1H), 4.67 – 4.54 (m, 1H), 4.49 – 4.35 (m, 1H), 2.93 – 2.68 (m, 2H), 1.61 – 1.36 (m, 2H), 1.23 – 1.15 (m, 1H), 0.91 – 0.84 (m, 3H), 0.81 – 0.74 (m, 3H). ^{13}C NMR (101 MHz, DMSO-*d$_6$*) δ 171.34, 166.36, 164.61, 142.36, 138.83, 137.99, 134.98, 129.43, 129.24, 128.95, 128.11, 127.49, 126.16, 124.14, 122.21, 51.07, 50.95, 41.31, 39.00, 24.16, 22.94, 21.69. ESI-MS [M + Na]$^+$ = 456.3. HPLC t$_R$ = 8.11 min and 8.54 min (*E/Z* mixture).

N-((S)-1-(((S)-5-Amino-5-oxo-1-phenylpent-3-en-2-yl)amino)-4-methyl-1-oxopentan-2-yl)-1H-indole-2-carboxamide (13b). This product was obtained by reacting **9b** (196 mg, 0.5 mmol) with diethyl (2-amino-2-oxoethyl)phosphonate (146 mg, 0.75 mmol) according to procedure I. Flash purification with CH$_2$Cl$_2$/MeOH (0 - 7% MeOH). Yield: 100 mg (47%) of **13b** as a white solid. Mp: 111-112 °C. ^{1}H NMR (400 MHz, DMSO-*d$_6$*) δ 11.61 – 11.53 (m, 1H), 8.38 – 8.28 (m, 1H), 8.22 (d, *J* = 8.6 Hz, 1H), 7.65 – 7.58 (m, 1H), 7.46 – 7.40 (m, 1H), 7.38 (d, *J* = 8.9 Hz, 1H), 7.28 – 7.24 (m, 1H), 7.24 – 7.19 (m, 4H), 7.19 – 7.17 (m, 1H), 7.17 – 7.11 (m, 1H), 7.07 – 7.01 (m, 1H), 7.00 – 6.94 (m, 1H), 6.66 – 6.53 (m, 1H), 6.01 – 5.82 (m, 1H), 4.68 – 4.43 (m, 2H), 2.93 – 2.70 (m, 2H), 1.71 – 1.60 (m, 1H), 1.51 – 1.34 (m, 2H), 0.93 – 0.86 (m, 3H), 0.85 – 0.80 (m, 3H). ^{13}C NMR (101 MHz, DMSO-*d$_6$*) δ 171.48, 166.32, 160.84, 142.38, 137.95, 136.41, 131.35, 129.26, 128.03, 127.03, 126.13, 124.18, 123.33, 121.51, 119.66, 112.20, 103.41, 51.40, 50.98, 40.58, 39.63, 24.29, 22.96, 21.48. ESI-MS [M + Na]$^+$ = 469.4. HPLC t$_R$ = 8.08 min and 8.45 min (*E/Z* mixture).

(S)-2-Cinnamamido-N-((S)-4-cyano-1-phenylbut-3-en-2-yl)-4-methylpentanamide (14a). This product was obtained from **13a** (431 mg, 1 mmol) according to the procedure E. Flash purification with CH$_2$Cl$_2$/MeOH (0 - 7% MeOH). Yield: 338 mg (81%) of **14a** as a white solid. Mp: 74-75 °C. ^{1}H NMR (400 MHz, CDCl$_3$) δ 7.65 – 7.58 (m, 1H), 7.52 – 7.44 (m, 2H), 7.39 – 7.37 (m, 1H), 7.35 – 7.28 (m, 2H), 7.24 – 7.13 (m, 3H), 7.12

– 7.08 (m, 1H), 6.93 (d, J = 8.6 Hz, 1H), 6.71 – 6.63 (m, 1H), 6.55 (d, J = 15.0 Hz, 1H), 6.48 – 6.35 (m, 1H), 6.23 (d, J = 15.0 Hz, 1H), 5.57 – 5.41 (m, 1H), 4.93 – 4.80 (m, 1H), 4.63 – 4.43 (m, 1H), 3.01 – 2.81 (m, 2H), 1.77 – 1.73 (m, 1H), 1.32 – 1.24 (m, 2H), 0.96 (d, J = 6.5 Hz, 3H), 0.86 (d, J = 6.5 Hz, 3H). 0.86 (d, J = 6.5 Hz, 3H). ^{13}C NMR (101 MHz, CDCl$_3$) δ 171.94, 166.49, 153.39, 142.45, 135.73, 134.51, 130.31, 129.32, 129.12, 128.90, 128.06, 127.35, 119.78, 116.92, 100.56, 52.47, 51.99, 40.59, 40.19, 25.00, 22.97, 22.31. ESI-MS [M - H]$^-$ = 414.2. HPLC t_R = 8.46 min and 8.63 min (E/Z mixture).

N-((S)-1-(((S)-4-Cyano-1-phenylbut-3-en-2-yl)amino)-4-methyl-1-oxopentan-2-yl)-1H-indole-2-carboxamide (**14b**). This product was obtained from **13b** (453 mg, 1 mmol) according to procedure E. Flash purification with CH$_2$Cl$_2$/MeOH (0 - 7% MeOH). Yield: 406 mg (50%) of **14b** as a white solid. Mp: 91-92 °C. ^{1}H NMR (400 MHz, CDCl$_3$) δ 9.77 – 9.42 (m, 1H), 7.71 – 7.57 (m, 1H), 7.49 – 7.38 (m, 1H), 7.36 – 7.29 (m, 1H), 7.29 – 7.20 (m, 2H), 7.20 – 7.09 (m, 3H), 7.09 – 7.00 (m, 2H), 6.98 – 6.91 (m, 1H), 6.86 – 6.68 (m, 1H), 6.67 – 6.57 (m, 1H), 5.55 – 5.40 (m, 1H), 4.95 – 4.82 (m, 1H), 4.65 – 4.47 (m, 1H), 2.93 – 2.75 (m, 2H), 1.79 – 1.68 (m, 1H), 1.61 – 1.50 (m, 1H), 1.46 – 1.37 (m, 1H), 0.97 – 0.88 (m, 3H), 0.86 – 0.79 (m, 3H). ^{13}C NMR (101 MHz, CDCl$_3$) δ 171.87, 162.29, 153.34, 136.68, 135.74, 129.64, 129.21, 128.93, 127.56, 127.24, 125.23, 122.30, 121.10, 117.19, 112.22, 103.93, 100.51, 52.48, 51.83, 40.51, 39.98, 24.99, 22.83, 22.27. ESI-MS [M + Na]+ = 451.3. HPLC t_R = 8.80 min and 8.95 min (E/Z mixture).

3.2. Enzymatic Assays. *General information*. Spectrophotometric assays were carried out on a Varian Cary 50 Bio in cuvettes. Fluorometric assays were performed on a FLUOstar Optima plate reader (BMG Labtech) in 96-well plates. Human CatL was purchased from Enzo Life Sciences, human CatB from Calbiochem (Merck), and human CatS from Enzo Life Sciences. All substrates were purchased from Bachem. The inhibitor stock solutions were prepared in DMSO. The progress curves were analyzed by linear regression. K_i values were obtained from duplicate measurements with five different inhibitor concentrations and analyzed by non-linear regression using the equation $v = v_0/(1 + [I]/(K_i \times (1 + [S]/K_m))$, where v and v_0 are the product formation rates in the presence and absence of inhibitor, [S] is the substrate concentration, and K_m is the Michaelis constant.

Cathepsin L.[35,36] The enzyme stock solution (20 mM malonate buffer pH 5.5, 400 mM NaCl, and 1 mM EDTA) was diluted 1:100 with assay buffer (100 mM sodium phosphate buffer pH 6.0, 100 mM NaCl, 5 mM EDTA, and 0.01% (w/v) Brij 35) containing 5 mM DTT, incubated at 37 °C for 30 min, and then stored on ice. A 10 mM solution of the substrate Z-Phe-Arg-pNA was prepared in DMSO. In a cuvette containing 940 μL assay buffer, the chromogenic substrate (10 μL) and DMSO and/or inhibitor solution (10 μL) was pipetted. Upon addition of CatL (40 μL), the measurement was started and followed at 37 °C for 60 min at 405 nm. The final substrate concentration was 100 μM (= 5.88 × K_m), and the final DMSO concentration was 2% (v/v).

Cathepsin B.[37] The enzyme stock solution (in 20 mM sodium acetate buffer pH 5.5, containing 1 mM EDTA) was diluted 1:500 with assay buffer (100 mM sodium phosphate buffer pH 6.0, 100 mM NaCl, 5 mM EDTA, and 0.01% (w/v) Brij 35) containing 5 mM DTT, incubated at 37 °C for 30 min, and then stored on ice. A 100 mM solution of the substrate Z-Arg-Arg-pNA was prepared in DMSO. Into a cuvette containing 950 μL assay buffer, the chromogenic substrate (5 μL) and DMSO and/or inhibitor solution (15 μL) was pipetted. Upon addition of CatB (30 μL), the measurement was started and followed at 37 °C for 60 min at 405 nm. The final substrate concentration was 500 μM (= 0.45 × K_m), and the final DMSO concentration was 2% (v/v).

Cathepsin S. The enzyme stock solution (in 100 mM MES, pH 6.5, containing 1 mM EDTA, 50 mM L-cysteine, 10 mM DTT, 0.5% Triton X-100, and 30% glycerol) was diluted 1:100 with assay buffer (50 mM sodium phosphate buffer, pH 6.5, 50 mM NaCl, 2 mM EDTA, 0.01% Triton X-100) containing 5 mM DTT, incubated at 37°C for 60 min, and then stored on ice. A 10 mM solution of the substrate Bz-Phe-Val-Arg-pNA was prepared in DMSO. In a cuvette containing 215 μL assay buffer, the chromogenic substrate (1.75 μL) and DMSO and/or inhibitor solution (3.25 μL) were pipetted. Upon addition of CatS (30 μL), the measurement was started and followed at 37 °C for 60 min at 405 nm. The final substrate concentration was 70 μM (= 1.13 × K_m), and the final DMSO concentration was 2% (v/v). A K_m value of 61.9 ± 11.4 μM for the CatS-catalyzed cleavage of Bz-Phe-Val-Arg-pNA was obtained from quadruplicate measurements with 13 different substrate concentrations. The standard error refers to the non-linear regression.

SARS-CoV-2 M^{pro}. The enzyme was expressed and purified as previously described.[10] The assay was performed at 37 °C with an excitation wavelength of 360 nm and an emission wavelength of 460 nm. The total volume per well was 50 μL. The assay buffer was 50 mM MOPS, pH 7.2 containing 10 mM NaCl, 1 mM EDTA, and 0.01% Triton X-100. The substrate Boc-Abu-Tle-Leu-Gln-AMC was prepared as a 2.5 mM stock solution in DMSO. The substrate stock solution was diluted 1+23 with assay buffer and pipetted into a well containing 1 μL of inhibitor solution. This mixture was kept at 37 °C for 5 min. A volume of 1 μL of an enzyme-containing solution was diluted 1+24 with assay buffer and added to start the reaction, which was monitored for 60 min. The final substrate concentration was 50 μM (= 1.03 K_m), and the final DMSO content was 4% (v/v).

3.3. Cytotoxicity. *Cell culture*. Calu-3 cells (human lung, ATCC Cat# HTB-55) were maintained in Dulbecco's modified Eagle medium (DMEM)/F-12 supplemented with 10% FCS and 10 mM sodium pyruvate. The cell line was incubated at 37 °C and 5% CO$_2$ in a humidified atmosphere.

Cell vitality assay. To determine the cell vitality of Calu-3 cells treated with inhibitors, the CellTiter-Glo Luminescent Cell Viability Assay Kit (Promega) was used. Cells were grown in 96-well plates until reaching 50–60% confluency before they were incubated with DMSO (solvent control) or test compounds at a concentration of 10 μM for 24 h. Next, cell culture supernatants were removed, and 50 μL of the CellTiter-Glo substrate was added to each well and incubated for 30 min on a rocking platform. Finally, samples were transferred into white 96-well plates, and luminescence was measured using a Hidex Sense plate luminometer (Hidex).

3.4. Antiviral Activity. All work with infectious SARS-CoV-2 was conducted under BSL-3 conditions at the German Primate Centre, Göttingen/Germany. Calu-3 cells were grown in 48-well plates until reaching approx. 70% confluency. Cells

18

were incubated with 10-fold serial dilutions (10-0.001 µM) of inhibitors for 1 h at 37 °C prior to infection. Next, the inhibitor-containing cell culture supernatant was removed, and cells were infected with SARS-CoV-2 isolate NK, Pango lineage B.1.513, at an MOI of 0.01 in an inoculum volume of 400 µL for 1 h at 37 °C. At 1 h *p.i.*, the inoculum was removed, and cells were washed with PBS three times and further incubated in cell culture medium containing the respective inhibitor. Virus-containing supernatants were harvested 24 h *p.i.* and stored at −80 °C until further usage. To determine viral titers, confluently grown Vero E6 cells were inoculated for 1 h at 37 °C with 10-fold serial dilutions of virus-containing supernatants. Next, the inoculum was removed, and cells were washed once with PBS before they were overlaid with 1% plaque agarose (Biozym) dissolved in Eagle's minimal essential medium without phenol red (Lonza) and further incubated. At 48 h *p.i.*, virus-induced plaques were counted, and viral titers were determined as PFU/mL.

3.5. Stability in the Presence of Glutathione. The GSH stability test was performed using a previously described method.[49,50] For this purpose, a suitable HPLC method was applied that allowed sampling by injection every 20 min. To achieve the desired final inhibitor concentration of 10 µM, as well as a GSH concentration of 5 mM in a final volume of 1 mL, 1 µL of the inhibitor stock solution (10 mM), was added to 949 µL of phosphate buffer (pH 7.4) and 50 µL of the GSH stock solution (100 mM). The mixture was appropriately vortexed and subjected to HPLC. The autosampler was set to a temperature of 37 °C and 13 replicate measurements over 4 h were performed. The potential reaction of the inhibitor with GSH was monitored by comparing the decreasing area under the curve (AUC) of each compound. This was subsequently plotted graphically as percentage inhibitor concentration versus time.

3.6. Microsomal Metabolic Stability Studies. Pooled liver microsomes from male mice were purchased from Xenotech. Compound incubations were performed in the presence of an NADPH-regenerating system (5 mM glucose-6-phosphate, 5 U/mL glucose-6-phosphate dehydrogenase, and 1 mM $NADP^+$). The mouse liver microsomes (1 mg/mL), the NADPH-regenerating system, and 4 mM $MgCl_2 \times 6\ H_2O$ in 0.1 M Tris buffer (pH 7.4) were preincubated for 5 min at 37 °C and 750 rpm on a shaker. The reaction was started by adding the preheated compound. The reaction was quenched at selected time points (0, 10, 20, 30, 60, and 120 min) by pipetting 50 µL of reaction mix into 100 µL ice cold internal standard (50 µM) in acetonitrile. The samples were mixed and centrifuged (1000 relative centrifugal force/4 °C/15 min). The supernatant was directly used for LC-MS analysis. All incubations were conducted in triplicate, and a limit of 1% organic solvent was not exceeded.

3.7. Pharmacokinetic Studies. The plasma stability assay, the metabolic stability assay, and the plasma protein binding assay were conducted as described previously.[51] For the HPLC-MS measurements, samples were analyzed using an Agilent 1290 Infinity II HPLC system coupled to an AB Sciex QTrap 6500plus or an AB Sciex Qtrap7500 mass spectrometer. LC conditions were as follows: column: Agilent Zorbax Eclipse Plus C18, 50×2.1 mm, 1.8 µm; temperature: 30 °C; injection volume: 5 µL per sample; flow rate: 700 µL min⁻¹.

Chromatograms were run under acidic conditions with solvents A (water + 0.1% formic acid) and B (95% acetonitrile/5% H_2O + 0.1% formic acid). The following gradient was applied: 99% A (1% B) at 0 min, 99–0% A (1–100% B) from 1.0 min to 4.0 min, 0% A (100% B) until 4.5 min, and 0-99% A (100–1% B) from 4.5 to 4.7 min.

3.8. Molecular Modeling. We virtually screened our in-house TüKIC library against Mᵖʳᵒ. This collection contains over 10,000 compounds targeting a variety of kinases. This library was previously prepared according to literature.[38] The CatL protein structure was prepared from the PDB 2XU3[45] (Resolution: 0.90 Å) using the Protein Wizard Preparation tool with standard options. All water molecules from the original PDB were removed for docking but placed back for later MD simulations. For the virtual screening we used molecular docking, carried out with Glide SP (version 9.1).[52] Grids were centered at the central point of the co-crystallized ligand. The top 500 hits, ranked by docking score, were visually inspected by observing the interaction with relevant residues and if reactive moieties would be near the catalytic cysteine.

To generate the potential binding mode of our hit ligands, we used covalent docking followed by long MD simulations. Briefly, three-dimensional ligand structures (**11g** and **9b**) were generated with LigPrep, using Epik to predict their protonation at pH 7.0 ± 1.0, and diastereoisomeric configurations were derived from the synthesis. The OPLS4 force field was employed for structure generation. Covalent docking was performed with CovDock[53] using Cys25 as an anchor, considering nucleophilic addition to the double bond or triple bond of the aldehyde or nitrile groups as reaction type. For each ligand, up to 10 poses were generated. Poses were selected according to the docking score and relevant interactions.

MD simulations were carried out by using the Desmond engine[54] with the OPLS4 force field.[55] The system encompassed the protein-ligand/cofactor complex, a predefined water model (TIP3P)[56] as a solvent, and counterions (Na⁺ or Cl⁻ adjusted to neutralize the overall system charge). The system was treated in a cubic box with a periodic boundary condition (PBC) specifying the shape and size of the box as 13 Å distance from the box edges to any atom of the protein. Short-range coulombic interactions were calculated using 1 fs time steps and 9.0 Å cut-off value, whereas long-range coulombic interactions were estimated using the Smooth Particle Mesh Ewald (PME) method.[57] Each system generated from CatL and the ligand was subjected to at least 5 µs simulations (five replicas of 1 µs each) with random seeds. Atomic interactions and distances were determined using the Simulation Event Analysis pipeline as implemented in Maestro 2021.4 (Schrödinger LCC) using standard options. Representative frames of the simulations were retrieved using hierarchical clustering analyses. Trajectories were clustered using the script trj_cluster.py (implemented in Maestro 2021.4, Schrödinger LCC) according to the root-mean-square deviation (RMSD) of ligand's heavy atoms, using 1 Å as a cut-off (see Figure S3). RMSD values of the protein backbone were used to monitor simulation equilibration and protein folding changes (see Figure S5) All the trajectory and interaction data are available on the Zenodo repository (code: 10.5281/zenodo.6984711). MD trajectories were visualized, and figures produced by PyMOL v.2.5.2 (Schrödinger LCC, New York, NY, USA).

19

ASSOCIATED CONTENT

Supporting Information

The Supporting Information is available at

GSH studies (Figure S1), metabolic stability studies (Figure S2, Table S1-S3), molecular modeling (Figure S3), ^{1}H & ^{13}C NMR spectra of representative compounds (Figure S4-S24) HPLC traces of representative compounds, a SMILES notation file (CSV)

AUTHOR INFORMATION

Corresponding Authors

Michael Gütschow − *PharmaCenter Bonn, Pharmaceutical Institute, Pharmaceutical & Medicinal Chemistry, University of Bonn, An der Immenburg 4, D-53121 Bonn, Germany; https://orcid.org/0000-0002-9376-7897; E-mail: guetschow@uni-bonn.de*

Thanigaimalai Pillaiyar − *Department of Pharmaceutical and Medicinal Chemistry, Institute of Pharmaceutical Sciences, Eberhard Karls Universität Tübingen, 72076 Tübingen, Germany; Phone: +49 7071 2977458; https://orcid.org/0000-0001-5575-8896; E-mail: thanigaimalai.pillaiyar@uni-tuebingen.de*

Authors

Philipp Flury − *Institute of Pharmacy, Pharmaceutical/ Medicinal Chemistry and Tübingen Center for Academic Drug Discovery, Eberhard Karls University Tübingen, Auf der Morgenstelle 8, 72076 Tübingen, Germany.*

Julian Breidenbach − *PharmaCenter Bonn, Pharmaceutical Institute, Pharmaceutical & Medicinal Chemistry, University of Bonn, Bonn D-53121, Germany*

Nadine Krüger – *Platform Infection Models, German Primate Center, Leibniz Institute for Primate Research Göttingen, Göttingen 37077, Germany*

Rabea Voget − *PharmaCenter Bonn, Pharmaceutical Institute, Pharmaceutical & Medicinal Chemistry, University of Bonn, Bonn D-53121, Germany*

Laura Schäkel − *PharmaCenter Bonn, Pharmaceutical Institute, Pharmaceutical & Medicinal Chemistry, University of Bonn, Bonn D-53121, Germany*

Yaoyao Si − *PharmaCenter Bonn, Pharmaceutical Institute, Pharmaceutical & Medicinal Chemistry, University of Bonn, Bonn D-53121, Germany*

Vesa Krasniqi − *PharmaCenter Bonn, Pharmaceutical Institute, Pharmaceutical & Medicinal Chemistry, University of Bonn, Bonn D-53121, Germany*

Sara Calistri − *Institute of Pharmacy, Pharmaceutical/ Medicinal Chemistry and Tübingen Center for Academic Drug Discovery, Eberhard Karls University Tübingen, Auf der Morgenstelle 8, 72076 Tübingen, Germany.*

Matthias Olfert − *Institute of Pharmacy, Pharmaceutical (Bio-)Analysis Eberhard Karls University Tübingen, Auf der Morgenstelle 8, 72076 Tübingen, Germany.*

Katharina Sylvester − *PharmaCenter Bonn, Pharmaceutical Institute, Pharmaceutical & Medicinal Chemistry, University of Bonn, Bonn D-53121, Germany*

Cheila Rocha −*Infection Biology Unit, German Primate Center, Leibniz Institute for Primate Research Göttingen, Göttingen 37077, Germany*

Raphael Ditzinger − *Institute of Pharmacy, Pharmaceutical/ Medicinal Chemistry and Tübingen Center for Academic Drug Discovery, Eberhard Karls University Tübingen, Auf der Morgenstelle 8, 72076 Tübingen, Germany.*

Alex Rasch − *Institute of Pharmacy, Pharmaceutical/ Medicinal Chemistry and Tübingen Center for Academic Drug Discovery, Eberhard Karls University Tübingen, Auf der Morgenstelle 8, 72076 Tübingen, Germany.*

Stefan Pöhlmann − *Infection Biology Unit, German Primate Center, Leibniz Institute for Primate Research Göttingen, Kellnerweg 4, 37077 Göttingen, Germany: Faculty of Biology and Psychology, University Göttingen, Göttingen 37073, Germany*

Thales Kronenberger − *Institute of Pharmacy, Pharmaceutical/Medicinal Chemistry and Tübingen Center for Academic Drug Discovery, Eberhard Karls University Tübingen, Auf der Morgenstelle 8, 72076 Tübingen, Germany. Cluster of Excellence iFIT (EXC 2180) "Image-Guided & Functionally Instructed Tumor Therapies", University of Tübingen, Tübingen 72076, Germany. School of Pharmacy, University of Eastern Finland, Faculty of Health Sciences, Kuopio 70211, Finland*

Antti Poso − *Institute of Pharmacy, Pharmaceutical/Medicinal Chemistry and Tübingen Center for Academic Drug Discovery, Eberhard Karls University Tübingen, Auf der Morgenstelle 8, 72076 Tübingen, Germany. Cluster of Excellence iFIT (EXC 2180) "Image-Guided & Functionally. School of Pharmacy, University of Eastern Finland, Faculty of Health Sciences, Kuopio 70211, Finland*

Katharina Rox− *Department of Chemical Biology, Helmholtz Centre for Infection Research (HZI) and German Center for Infection Research (DZIF), Inhoffenstraße 7, 38124 Braunschweig, Germany; orcid.org/ 0000-0002-8020-1384*

Stefan A. Laufer − *Institute of Pharmacy, Pharmaceutical/ Medicinal Chemistry and Tübingen Center for Academic Drug Discovery, Eberhard Karls University Tübingen, Auf der Morgenstelle 8, 72076 Tübingen, Germany. Cluster of Excellence iFIT (EXC 2180) "Image-Guided & Functionally Instructed Tumor Therapies", University of Tübingen, Tübingen 72076, Germany; orcid.org/0000-0001-6952- 1486*

Christa E. Müller − *PharmaCenter Bonn, Pharmaceutical Institute, Pharmaceutical & Medicinal Chemistry, University of Bonn, Bonn D-53121, Germany; orcid.org/0000-0002- 0013-6624*

Author Contributions

T.P. conceived the study. P.F. and S.C. synthesized the compounds and performed structural analyses. J.B., R.V., L.S., Y.S., V.K., and K.S. performed biochemical experiments. N.K. and C.R. performed pharmacological experiments. T.K. performed computational studies. R.D., A.R., and K.R. performed ADME studies. All authors contributed to data analyses. A.P., S.P., S.L., C.E.M., M.G., and T.P. supervised

20

the project. P.F., J.B., M.G., and T.P. wrote the manuscript with contributions from all coauthors. All authors have given approval to the final version of the manuscript.

REFERENCES

(1) Hoffmann, M., Krüger, N., Schulz, S., Cossmann, A., Rocha, C., Kempf, A., Nehlmeier, I., Graichen, L., Moldenhauer, A. S., Winkler, M. S., Lier, M., Dopfer-Jablonka, A., Jäck, H. M., Behrens, G. M. N., Pöhlmann, S. (2022) The Omicron variant is highly resistant against antibody-mediated neutralization: Implications for control of the Covid-19 pandemic. *Cell 185*, 447–456. DOI: 10.1016/j.cell.2021.12.032.

(2) Pillaiyar, T., Wendt, L. L., Manickam, M., Easwaran, M. (2021) The recent outbreaks of human coronaviruses: A medicinal chemistry perspective. *Med. Res. Rev. 41*, 72–135. DOI: 10.1002/med.21724.

(3) Gil, C., Ginex, T., Maestro, I., Nozal, V., Barrado-Gil, L., Cuesta-Geijo, M. Á., Urquiza, J., Ramírez, D., Alonso, C., Campillo, N. E., Martinez, A. (2020) Covid-19: Drug targets and potential treatments. *J. Med. Chem. 63*, 12359–12386. DOI: 10.1021/acs.jmedchem.0c00606.

(4) Herrmann, L., Hahn, F., Wangen, C., Marschall, M., Tsogoeva, S. B. (2022) Anti-SARS-CoV-2 inhibitory profile of new quinoline compounds in cell culture-based infection models. *Chem. Eur. J. 28*, e202103861. DOI: 10.1002/chem.202103861.

(5) Brevini, T., Maes, M., Webb, G. J., John, B. V., Fuchs, C. D., Buescher, G., Wang, L., Griffiths, C., Brown, M. L., Scott, W. E., Pereyra-Gerber, P., Gelson, W. T. H., Brown, S., Dillon, S., Muraro, D., Sharp, J., Neary, M., Box, H., Tatham, L., Stewart, J., Curley, P., Pertinez, H., Forrest, S., Mlcochova, P., Varankar, S. S., Darvish-Damavandi, M., Mulcahy, V. L., Kuc, R. E., Williams, T. L., Heslop, J. A., Rossetti, D., Tysoe, O. C., Galanakis, V., Vila-Gonzalez, M., Crozier, T. W. M., Bargehr, J., Sinha, S., Upponi, S. S., Fear, C., Swift, L., Saeb-Parsy, K., Davies, S. E., Wester, A., Hagström, H., Melum, E., Clements, D., Humphreys, P., Herriott, J., Kijak, E., Cox, H., Bramwell, C., Valentijn, A., Illingworth, C. J. R., UK-PBC Consortium, Dahman, B., Bastaich, D. R., Ferreira, R. D., Marjot, T., Barnes, E., Moon, A. M., Barritt, A. S. 4th, Gupta, R. K., Baker, S., Davenport, A. P., Corbett, G., Gorgoulis, V. G., Buczacki, S. J. A., Lee, J. H., Matheson, N. J., Trauner, M., Fisher, A. J., Gibbs, P., Butler, A. J., Watson, C. J. E., Mells, G. F., Dougan, G., Owen, A., Lohse, A. W., Vallier, L., Sampaziotis, F. (2023) FXR inhibition may protect from SARS-CoV-2 infection by reducing ACE2. *Nature 615*, 134–142. DOI: 10.1038/s41586-022-05594-0.

(6) McCreary, E. K., Angus, D. C. (2020) Efficacy of Remdesivir in Covid-19. *JAMA 324*, 1041–1042. DOI: 10.1001/jama.2020.16337.

(7) Pagliano, P., Sellitto, C., Ascione, T., Scarpati, G., Folliero, V., Piazza, O., Franci, G., Filippelli, A., Conti, V. (2022) The preclinical

discovery and development of Molnupiravir for the treatment of Sars-Cov-2 (Covid-19). *Expert Opin. Drug Discov. 17*, 1299–1311. DOI: 10.1080/17460441.2022.2153828.

(8) Cheema, H. A., Jafar, U., Sohail, A., Shahid, A., Sahra, S., Ehsan, M., Athar, F., Shah, J., Sah, R. (2023) Nirmatrelvir-Ritonavir for the treatment of Covid-19 patients: A systematic review and meta-analysis. *J. Med. Virol. 95*, e28471. DOI: 10.1002/jmv.28471.

(9) Bai, B., Arutyunova, E., Khan, M. B., Lu, J., Joyce, M. A., Saffran, H. A., Shields, J. A., Kandadai, A. S., Belovodskiy, A., Hena, M., Vuong, W., Lamer, T., Young, H. S., Vederas, J. C., Tyrrell, D. L., Lemieux, M. J., Nieman, J. A. (2021) Peptidomimetic nitrile warheads as Sars-CoV-2 3CL protease inhibitors. *RSC Med. Chem. 12*, 1722–1730. DOI: 10.1039/D1MD00247C.

(10) Breidenbach, J., Lemke, C., Pillaiyar, T., Schäkel, L., Al Hamwi, G., Diett, M., Gedschold, R., Geiger, N., Lopez, V., Mirza, S., Namasivayam, V., Schiedel, A. C., Sylvester, K., Thimm, D., Vielmuth, C., Phuong Vu, L., Zyulina, M., Bodem, J., Gütschow, M., Müller, C. E. (2021) Targeting the Main Protease of SARS-CoV-2: From the establishment of high throughput screening to the design of tailored inhibitors. *Angew. Chem. Int. Ed. 60*, 10423–10429. DOI: 10.1002/anie.202016961.

(11) Zhang, C.-H., Stone, E. A., Deshmukh, M., Ippolito, J. A., Ghahremanpour, M. M., Tirado-Rives, J., Spasov, K. A., Zhang, S., Takeo, Y., Kudalkar, S. N. (2021) Potent noncovalent inhibitors of the Main Protease of SARS-CoV-2 from molecular sculpting of the drug perampanel guided by free energy perturbation calculations. *ACS Cent. Sci. 7*, 467–475. DOI: 10.1021/acscentsci.1c00039.

(12) Dai, W., Zhang, B., Jiang, X.-M., Su, H., Li, J., Zhao, Y., Xie, X., Jin, Z., Peng, J., Liu, F. (2020) Structure-based design of antiviral drug candidates targeting the SARS-CoV-2 Main Protease. *Science 368*, 1331–1335. DOI: 10.1126/science.abb4489.

(13) Qiao, J., Li, Y. S., Zeng, R., Liu, F. L., Luo, R.-H., Huang, C., Wang, Y. F., Zhang, J., Quan, B., Shen, C., Mao, X., Liu, X., Sun, W., Yang, W., Ni, X., Wang, K., Xu, L., Duan, Z. L., Zou, Q. C., Zhang, H. L., Qu, W., Long, Y. H.-P., Li, M. H., Yang, R. C., Liu, X., You, J., Zhou, Y., Yao, R., Li, W. P., Liu, J. M., Chen, P., Liu, Y., Lin, G. F., Yang, X., Zou, J., Li, L., Hu, Y., Lu, G. W., Li, W. M., Wei, Y. Q., Zheng, Y. T., Lei, J., Yang, S. (2021) Sars-Cov-2 Mpro inhibitors with antiviral activity in a transgenic mouse model. *Science 371*, 1374–1378. DOI: 10.1126/science.abf1611.

(14) Gao, K., Wang, R., Chen, J., Tepe, J. J., Huang, F., Wei, G.-W. (2021) Perspectives on SARS-CoV-2 main protease inhibitors. *J. Med. Chem. 64*, 16922–16955. DOI: 10.1021/acs.jmedchem.1c00409.

(15) Gao, K., Sylvester, K., Song, L., Claff, T., Jing, L., Woodson, M., Weiße, R. H., Cheng, Y., Schäkel, L., Petry, M., Gütschow, M., Schiedel, A. C., Sträter, N., Kang, D., Xu, S., Toth, K., Tavis, J., Tollefson, A. E., Müller, C. E., Liu, X., Zhan, P. (2022) Discovery and crystallographic studies of trisubstituted piperazine derivatives as non-covalent SARS-CoV-2 main protease inhibitors with high target specificity and low toxicity. *J. Med. Chem. 65*, 13343–13364. DOI: 10.1021/acs.jmedchem.2c01146.

(16) Dampalla, C. S., Rathnayake, A. D., Galasiti Kankanamalage, A. C., Kim, Y., Perera, K. D., Nguyen, H. N., Miller, M. J., Madden, T. K., Picard, H. R., Thurman, H. A., Kashipathy, M. M., Liu, L., Battaile, K. P., Lovell, S., Chang, K. O., Groutas, W. C. (2022) Structure-guided design of potent spirocyclic inhibitors of severe acute respiratory syndrome coronavirus-2 3C-like protease. *J. Med. Chem. 65*, 7818–7832. DOI: 10.1021/acs.jmedchem.2c00224.

(17) Dampalla, C. S., Nguyen, H. N., Rathnayake, A. D., Kim, Y., Perera, K. D., Madden, T. K., Thurman, H. A., Machen, A. J., Kashipathy, M. M., Liu, L., Battaile, K. P., Lovell, S., Chang, K. O., Groutas, W. C. (2022) Broad-spectrum cyclopropane-based inhibitors of coronavirus 3C-like proteases: Biochemical, structural, and virological studies. *ACS Pharmacol. Transl. Sci. 6*, 181–194. DOI: 10.1021/acsptsci.2c00206.

(18) Ren, L. L., Wang, Y. M., Wu, Z. Q., Xiang, Z. C., Guo, L., Xu, T., Jiang, Y. Z., Xiong, Y., Li, Y. J., Li, X. W., Li, H., Fan, G. H., Gu, X. Y., Xiao, Y., Gao, H., Xu, J. Y., Yang, F., Wang, X. M., Wu, C., Chen, L., Liu, Y. W., Liu, B., Yang, J., Wang, X. R., Dong, J., Li, L.,

Huang, C. L., Zhao, J. P., Hu, Y., Cheng, Z. S., Liu, L. L., Qian, Z. H., Qin, C., Jin, Q., Cao, B., Wang, J. W. (2020) Identification of a novel coronavirus causing severe pneumonia in human: A descriptive study. *Chin. Med. J. (Engl.) 133*, 1015–1024. DOI: 10.1097/cm9.0000000000000722.

(19) Shang, J., Wan, Y., Luo, C., Ye, G., Geng, Q., Auerbach, A., Li, F. (2020) Cell entry mechanisms of SARS-CoV-2. *Proc. Natl. Acad. Sci. 117*, 11727–11734. DOI: 10.1073/pnas.2003138117.

(20) Letko, M., Marzi, A., Munster, V. (2020) Functional assessment of cell entry and receptor usage for Sars-Cov-2 and other lineage B betacoronaviruses. *Nat. Microbiol. 5*, 562–569. DOI: 10.1038/s41564-020-0688-y.

(21) Hoffmann, M., Kleine-Weber, H., Schroeder, S., Krüger, N., Herrler, T., Erichsen, S., Schiergens, T. S., Herrler, G., Wu, N. H., Nitsche, A. (2020) SARS-CoV-2 cell entry depends on Ace2 and TMPRSS2 and is blocked by a clinically proven protease inhibitor. *Cell 181*, 271–280. DOI: 10.1016/j.cell.2020.02.052.

(22) Ou, X., Liu, Y., Lei, X., Li, P., Mi, D., Ren, L., Guo, L., Guo, R., Chen, T., Hu, J., Xiang, Z., Mu, Z., Chen, X., Chen, J., Hu, K., Jin, Q., Wang, J., Qian, Z. (2020) Characterization of spike glycoprotein of SARS-CoV-2 on virus entry and its immune cross-reactivity with Sars-Cov. *Nat. Commun. 11*, 1620. DOI: 10.1038/s41467-020-15562-9.

(23) Pišlar, A., Mitrović, A., Sabotič, J., Pečar Fonović, U., Perišić Nanut, M., Jakoš, T., Senjor, E., Kos, J. (2020) The role of cysteine peptidases in coronavirus cell entry and replication: The therapeutic potential of cathepsin inhibitors. *PLoS Pathog. 16*, e1009013. DOI: 10.1371/journal.ppat.1009013.

(24) Mellott, D. M., Tseng, C.-T., Drelich, A., Fajtová, P., Chenna, B. C., Kostomiris, D. H., Hsu, J., Zhu, J., Taylor, Z. W., Kocurek, K. I. (2021) A clinical-stage cysteine protease inhibitor blocks SARS-CoV-2 infection of human and monkey cells. *ACS Chem. Biol. 16*, 642650. DOI: 10.1021/acschembio.0c00875.

(25) Ashhurst, A. S., Tang, A. H., Fajtová, P., Yoon, M. C., Aggarwal, A., Bedding, M. J., Stoye, A., Beretta, L., Pwee, D., Drelich, A. (2021) Potent anti-Sars-Cov-2 activity by the natural product gallinamide a and analogues via inhibition of cathepsin L. *J. Med. Chem. 65*, 2956–2970. DOI: 10.1021/acs.jmedchem.1c01494.

(26) Scarcella, M., d'Angelo, D., Ciampa, M., Tafuri, S., Avallone, L., Pavone, L. M., De Pasquale, V. (2022) The key role of lysosomal protease cathepsins in viral infections. *Int. J. Mol. Sci. 23*, 9089. DOI: 10.3390/ijms23169089.

(27) Zhao, S., Jiang, M., Qing, H., Ni, J. (2023) Cathepsins and SARS-CoV-2 infection: From pathogenic factors to potential therapeutic targets. *Br. J. Pharmacol. 180*, 2455–2481.

(28) Zhao, M. M., Yang, W. L., Yang, F. Y., Zhang, L., Huang, W. J., Hou, W., Fan, C. F., Jin, R. H., Feng, Y. M., Wang, Y. C., Yang, J. K. (2021) Cathepsin L plays a key role in Sars-Cov-2 infection in humans and humanized mice and is a promising target for new drug development. *Signal Transduct. Target. Ther. 6*, 134. DOI: 10.1038/s41392-021-00558-8.

(29) Coomes, E. A., Haghbayan, H. (2020) Interleukin-6 in Covid-19: A systematic review and meta-analysis. *Rev. Med. Virol. 30*, 1–9. DOI: 10.1002/rmv.2141.

(30) Meng, B., Abdullahi, A., Ferreira, I., Goonawardane, N., Saito, A., Kimura, I., Yamasoba, D., Gerber, P. P., Fatihi, S., Rathore, S., Zepeda, S. K., Papa, G., Kemp, S. A., Ikeda, T., Toyoda, M., Tan, T. S., Kuramochi, J., Mitsunaga, S., Ueno, T., Shirakawa, K., Takaori-Kondo, A., Brevini, T., Mallery, D. L., Charles, O. J., Bowen, J. E., Joshi, A., Walls, A. C., Jackson, L., Martin, D., Smith, K. G. C., Bradley, J., Briggs, J. A. G., Choi, J., Madissoon, E., Meyer, K. B., Mlcochova, P., Ceron-Gutierrez, L., Doffinger, R., Teichmann, S. A., Fisher, A. J., Pizzuto, M. S., de Marco, A., Corti, D., Hosmillo, M., Lee, J. H., James, L. C., Thukral, L., Veesler, D., Sigal, A., Sampaziotis, F., Goodfellow, I. G., Matheson, N. J., Sato, K., Gupta, R. K. (2022) Altered Tmprss2 usage by SARS-CoV-2 omicron impacts infectivity and fusogenicity. *Nature 603*, 706–714. DOI: 10.1038/s41586-022-04474-x.

(31) Zhu, W., Xu, M., Chen, C. Z., Guo, H., Shen, M., Hu, X., Shinn, P., Klumpp-Thomas, C., Michael, S. G., Zheng, W. (2020) Identification of SARS-CoV-2 3CL protease inhibitors by a quantitative high-throughput screening. *ACS Pharmacol. Transl. Sci. 3*, 1008–1016. DOI: 10.1021/acsptsci.0c00108.

(32) Jeong, J. H., Choi, J. H., Kim, B. K., Min, S. C., Chokkakula, S., Oh, S., Park, J. H., Shim, S. M., Kim, E. G., Choi, Y. K., Lee, J. Y., Baek, Y. H., Song, M. S. (2023) Evaluating Z-FA-FMK, a host cathepsin L protease inhibitor, as a potent and broad-spectrum antiviral therapy against SARS-CoV-2 and related coronaviruses. *Antiviral Res. 216*, 105669. DOI: 10.1016/j.antiviral.2023.105669.

(33) Reinke, P. Y., de Souza, E. E., Günther, S., Falke, S., Lieske, J., Ewert, W., Loboda, J., Herrmann, A., Rahmani Mashhour, A., Karničar, K., Usenik, A., Lindič, N., Sekirnik, A., Botosso, V. F., Santelli, G. M., Kapronezai, J., de Araújo. M. V., Silva-Pereira. T. T., Filho, A. F., Tavares. M. S., Flórez-Álvarez. L., de Oliveira. D. B., Durigon, E. L., Giaretta, P. R., Heinemann, M. B., Hauser, M., Seychell, B., Böhler, H., Rut, W., Drag, M., Beck, T., Cox, R., Chapman, H. N., Betzel, C., Brehm, W., Hinrichs, W., Ebert, G., Latham, S. L., Guimarães, A. M., Turk, D., Wrenger, C., Meents, A. (2023) Calpeptin is a potent cathepsin inhibitor and drug candidate for SARS-CoV-2 infections. *Commun. Biol. 6*, 1058. DOI: 10.1038/s42003-023-05317-9.

(34) Shie, J. J., Fang, J. M., Kuo, C. J., Kuo, T. H., Liang, P. H., Huang, H. J., Yang, W. B., Lin, C. H., Chen, J. L., Wu, Y. T., Wong, C. H. (2005) Discovery of potent anilide inhibitors against the severe acute respiratory syndrome 3CL protease. *J. Med. Chem. 48*, 4469–4473. DOI: 10.1021/jm050184y.

(35) Frizler, M., Lohr, F., Lülsdorff, M., Gütschow, M. (2011) Facing the *gem*-dialkyl effect in enzyme inhibitor design: Preparation of homocycloleucine-based azadipeptide mitriles. *Chem. Eur. J. 17*, 11419–11423. DOI: 10.1002/chem.201101350.

(36) Lemke, C., Benysek, J., Brajtenbach, D., Breuer, C., Jílková, A., Horn, M., Busa, M., Ulrychová, L., Illies, A., Kubatzky, K. F. (2021) An activity-based probe for cathepsin K imaging with excellent potency and selectivity. *J. Med. Chem. 64*, 13793–13806. DOI: 10.1021/acs.jmedchem.1c01178.

(37) Mertens, M. D., Schmitz, J., Horn, M., Furtmann, N., Bajorath, J., Mareš, M., Gütschow, M. (2014) A coumarin-labeled vinyl sulfone as tripeptidomimetic activity-based probe for cysteine cathepsins. *ChemBioChem 15*, 955–959. DOI: 10.1002/cbic.201300806.

(38) Pillaiyar, T., Flury, P., Krüger, N., Su, H., Schäkel, L., Barbosa Da Silva, E., Eppler, O., Kronenberger, T., Nie, T., Luedtke, S., Rocha, C., Sylvester, K., Petry, M. R. I., McKerrow, J. H., Poso, A., Pöhlmann, S., Gütschow, M., O'Donoghue, A. J., Xu, Y., Müller, C. E., Laufer, S. A. (2022) Small-molecule thioesters as Sars-Cov-2 Main Protease inhibitors: Enzyme inhibition, structure–activity relationships, antiviral activity, and X-Ray structure determination. *J. Med. Chem. 65*, 9376–9395. DOI: 10.1021/acs.jmedchem.2c00636.

(39) Cianni, L., Feldmann, C. W., Gilberg, E., Gütschow, M., Juliano, L., Leitão, A., Bajorath, J., Montanari, C. A. (2019) Can cysteine protease cross-class inhibitors achieve selectivity? *J. Med. Chem. 62*, 10497–10525. DOI: 10.1021/acs.jmedchem.9b00683.

(40) Hattori, S. I., Higashi-Kuwata, N., Hayashi, H., Allu, S. R., Raghavaiah, J., Bulut, H., Das, D., Anson, B. J., Lendy, E. K., Takamatsu, Y., Takamune, N., Kishimoto, N., Murayama, K., Hasegawa, K., Li, M., Davis, D. A., Kodama, E. N., Yarchoan, R., Wlodawer, A., Misumi, S., Mesecar, A. D., Ghosh, A. K., Mitsuya, H. (2021) A small molecule compound with an indole moiety inhibits the Main Protease of Sars-Cov-2 and blocks virus replication. *Nat. Commun. 12*, 668. DOI: 10.1038/s41467-021-20900-6.

(41) Choe, Y., Leonetti, F., Greenbaum, D. C., Lecaille, F., Bogyo, M., Brömme, D., Ellman, J. A., Craik, C. S.(2006) Substrate profiling of cysteine proteases using a combinatorial peptide library identifies functionally unique specificities. J. Biol. Chem. 281, 12824–12832. DOI: 10.1074/jbc.M513331200.

(42) Vizovišek, M., Vidmar, R., Van Quickelberghe, E., Impens, F., Andjelković, U., Sobotič, B., Stoka, V., Gevaert, K., Turk, B., Fonović, M. (2015) Fast profiling of protease specificity reveals similar substrate specificities for cathepsins K, L and S. P Proteomics 15, 2479–2490. DOI: 10.1002/pmic.201400460.

22

(43) Lemke, C., Cianni, L., Feldmann, C., Gilberg, E., Yin, J., dos Reis Rocho, F., de Vita, D., Bartz, U., Bajorath, J., Montanari, C. A., Gütschow, M. (2020) N-Sulfonyl dipeptide nitriles as inhibitors of human cathepsin S: In silico design, synthesis and biochemical characterization. *Bioorg. Med. Chem. Lett. 30*, 127420. DOI: 10.1016/j.bmcl.2020.127420.

(44) Masyeni, S., Iqhrammullah, M., Frediansyah, A., Nainu, F., Tallei, T., Emran, T. B., Ophinni, Y., Dhama, K., Harapan, H. (2022) Molnupiravir: A lethal mutagenic drug against rapidly mutating severe acute respiratory syndrome coronavirus 2—A narrative review. *J. Med. Virol. 94*, 3006–3016. DOI: 10.1002/jmv.27730.

(45) Hardegger, L. A., Kuhn, B., Spinnler, B., Anselm, L., Ecabert, R., Stihle, M., Gsell, B., Thoma, R., Diez, J., Benz, J., Plancher, J.-M., Hartmann, G., Banner, D. W., Haap, W., Diederich, F. (2011) Systematic investigation of halogen bonding in protein–ligand interactions. Angew. Chem. Int. Ed. 50, 314–318. DOI: 10.1002/anie.201006781.

(46) Dufour, E., Storer, A. C., Ménard, R. (1995) Peptide aldehydes and nitriles as transition state analog inhibitors of cysteine proteases. *Biochemistry 34*, 9136–9143. DOI: 10.1021/bi00028a024.

(47) Frizler, M., Stirnberg, M., Sisay, M. T., Gütschow, M. (2010) Development of nitrile-based peptidic inhibitors of cysteine cathepsins. *Curr. Top. Med. Chem. 10*, 294–322. DOI: 10.2174/156802610790725452.

(48) McKelvey, M. C., Abladey, A. A., Small, D. M., Doherty, D. F., Williams R., Scott, A., Spek, C. A., Borensztajn, K. S., Holsinger, L., Booth, R., O'Kane, C. M., McAuley, D. F., Taggart, C. C., Weldon, S. (2022) Cathepsin S contributes to lung inflammation in acute respiratory distress syndrome. *Am. J. Respir. Crit. Care Med. 205*, 769–782. DOI: 10.1164/rccm.202107-1631OC.

(49) Schmidt, T. J., Ak, M., Mrowietz, U. (2007) Reactivity of dimethyl fumarate and methylhydrogen fumarate towards glutathione and N-acetyl-L-cysteine - Preparation of S-substituted thiosuccinic acid esters. *Bioorg. Med. Chem. 2007, 15*, 333–342. DOI: 10.1016/j.bmc.2006.09.053

(50) Muth, F., El-Gokha, A., Ansideri, F., Eitel, M., Döring, E., Sievers-Engler, A., Lange, A., Boeckler, F. M., Lämmerhofer, M., Koch, P., Laufer, S. A. (2017) Tri- and tetrasubstituted pyridinylimidazoles as covalent inhibitors of C-Jun N-terminal kinase 3. *J. Med. Chem. 60*, 594–607. DOI: 10.1021/acs.jmedchem.6b01180.

(51) Mała, P., Siebs, E., Meiers, J., Rox, K., Varrot, A., Imberty, A., Titz, A. (2022) Discovery of N-B-L-fucosyl amides as high-affinity ligands for the *Pseudomonas Aeruginosa* lectin Lecb. *J. Med. Chem. 65*, 14180–14200. DOI: 10.1021/acs.jmedchem.2c01373.

(52) Halgren, T. A., Murphy, R. B., Friesner, R. A., Beard, H. S., Frye, L. L., Pollard, W. T., Banks, J. L. (2004) Glide: a new approach for rapid, accurate docking and scoring. 2. Enrichment factors in database screening. *J. Med. Chem. 47*, 1750–1759. DOI: 10.1021/jm030644s.

(53) Chu, X. Q., Zi, Y., Lu, X. M., Wang, S. Y., Ji, S. J. (2014) Intramolecular Pd-catalyzed C–H functionalization: Construction of fused tetracyclic bis-indole alkaloid analogues. *Tetrahedron 70*, 232–238. DOI: 10.1016/j.tet.2013.11.079.

(54) Bowers, K. J., Chow, D. E., Xu, H., Dror, R. O., Eastwood, M. P., Gregersen, B. A., Klepeis, J. L., Kolossvary, I., Moraes, M. A., Sacerdoti, F. D. (2006) In *Scalable algorithms for molecular dynamics simulations on commodity clusters*, SC'06: Proceedings of the 2006 ACM/IEEE Conference on Supercomputing, IEEE: 2006; pp 43–43.

(55) Lu, C., Wu, C., Ghoreishi, D., Chen, W., Wang, L., Damm, W., Ross, G. A., Dahlgren, M. K., Russell, E., Von Bargen, C. D., Abel, R., Friesner, R. A., Harder, E. D. (2021) Opls4: Improving force field accuracy on challenging regimes of chemical space. *J. Chem. Theory Comput. 17,* 4291–4300. DOI: 10.1021/acs.jctc.1c00302.

(56) Jorgensen, W. L., Chandrasekhar, J., Madura, J. D., Impey, R. W., Klein, M. L. (1983) Comparison of simple potential functions for simulating liquid water. *J. Chem. Phys. 79*, 926–935. DOI: 10.1063/1.445869.

(57) Darden, T., York, D., Pedersen, L. (1993) Particle Mesh Ewald: An N Log (N) method for Ewald sums in large systems. *J. Chem. Phys. 98*, 10089–10092. DOI: 10.1063/1.464397.

23

Table of Contents

Cathepsin-Targeting SARS-CoV-2 Inhibitors: Design, Synthesis, and Biological Activity

Philipp Flury, Julian Breidenbach, Nadine Krüger, Rabea Voget, Laura Schäkel, Yaoyao Si, Vesa Krasniqi, Sara Calistri, Matthias Olfert, Katharina Sylvester, Cheila Rocha, Raphael Ditzinger, Alex Rasch, Stefan Pöhlmann, Thales Kronenberger, Antti Poso, Katharina Rox, Stefan A. Laufer, Christa E. Müller, Michael Gütschow, and Thanigaimalai Pillaiyar

I (LN5053)
Cat L: K_i = 0.152 μM

11g
CatL: K_i = 0.00956 μM
CatS: K_i = 0.0169 μM
Calu-3 cells: EC_{50} = 2.70 μM

11e
CatL: K_i = 0.111 μM
CatS: K_i= 0.103 μM
Calu-3 cells: EC_{50} = 0.0351 μM

CatL-11g